

Scholar@UPRM

Structural changes of ^{13}C labelled ##### centrin and melittin upon complex formation in the presence of calcium

Item Type	Thesis
Authors	Del Valle Sosa, Liliana
Download date	2026-06-18 11:18:33
Link to Item	https://hdl.handle.net/20.500.11801/3818

Structural Changes of ^{13}C -labelled *Chlamydomonas* Centrin and Melittin Upon Complex Formation in the Presence of Calcium

by

Liliana del Valle Sosa

A thesis submitted in partial fulfillment of the requirements for the degree of

MASTER OF SCIENCE
in
CHEMISTRY

UNIVERSITY OF PUERTO RICO
MAYAGÜEZ CAMPUS
2006

Approved by:

Doris Ramírez, PhD
Member, Graduate Committee

Date

Jorge Ríos Steiner, PhD
Member, Graduate Committee

Date

Belinda Pastrana-Ríos, PhD
President, Graduate Committee

Date

Carlos Ríos Velázquez, PhD
Representative of Graduate Studies

Date

María Aponte, PhD
Chairperson of the Department

Date

ABSTRACT

Chlamydomonas centrin is an acidic, low molecular weight protein that belongs to the EF-hand superfamily of calcium binding proteins. It is an essential component of the centrosomal structure in a wide range of organisms. ^{13}C -labeled Chlamydomonas centrin ($^{13}\text{C-Cen}$) and a model peptide from bee venom, known as melittin (MLT) were studied upon complex formation. The main objective of this thesis was to study the level of protein/peptide interaction, to explore structural changes and the relative stability of centrin, mellitin, and the complex. Two sets of experiments were performed H \rightarrow D exchange via attenuated total reflectance (ATR) and thermal dependence via transmission Fourier transform-infrared (FT-IR) spectroscopy. The spectral analysis was carried-out by two-dimensional correlation analysis (2D-COS). In addition, differential scanning calorimetry (DSC) experiments were performed to corroborate the existence of pre-transitions and the thermal denaturation temperature for these proteins and the complex. For the FT-IR studies, the two protein components were studied simultaneously as: the amide I' band (1650 cm^{-1}) for MLT and the amide I*' band (1600 cm^{-1}) for $^{13}\text{C-Cen}$ in order to establish the structural changes during the interaction. Furthermore, the amide II band (1550 cm^{-1}) comprised of side chains and the N-H deformation mode, and the amide II' (1450 cm^{-1}) band comprised of the N-D deformation mode for both proteins are studied to determine side chain interaction and the extent of solvation (80% for $^{13}\text{C-Cen}$, 100% for MLT and 100% $^{13}\text{C-Cen/MLT}$). The interaction within the protein complex, was driven by

MLT, which was suggested from the effects observed in the α -helical motifs of centrin to a greater extent than its interaction with calcium. This effect was observed for the calorimetric studies whereby centrin pre-transition was shifted by 13 °C from 81 °C to 95 °C. Finally, these results provide the framework to study other centrin target peptides to further understand the biophysical and biochemical changes driving their interaction.

RESUMEN

Chlamydomonas centrina es una proteína ácida, de bajo peso molecular que pertenece a la superfamilia de proteínas de manos EF que enlazan calcio. Esta es un componente esencial de la estructura centrosomal de un amplio rango de organismos. La centrina de *Chlamydomonas* marcada con carbono 13 ($^{13}\text{C-Cen}$) y un péptido modelo del veneno de la abeja, conocido como meletina (MLT), fueron estudiados en la formación del complejo. El principal objetivo de esta tesis fue el estudio del nivel de interacción proteína/péptido, para examinar los cambios estructurales y la estabilidad relativa de centrina, meletina y la del complejo. Se realizaron dos tipos de experimentos: se estudió el intercambio H \rightarrow D a través de la reflectancia atenuada total (ATR) y luego, se analizó la dependencia termal utilizando la espectroscopía de transmisión de infrarrojo con transformada de Fourier (FT-IR) en la cuales los espectros se analizaron mediante el estudio de correlación en dos dimensiones (2D-COS). Además, se realizaron experimentos de calorimetría diferencial de barrido (DSC) para corroborar la existencia de pre-transiciones y la temperatura de desnaturalización termal de estas proteínas y el complejo. Para los estudios de FT-IR, los dos componentes proteicos fueron analizados simultáneamente como: la banda amida I' (1650 cm^{-1}) para MLT y la banda amida I*' (1600 cm^{-1}) para $^{13}\text{C-Cen}$ para los cambios estructurales durante la interacción. También, se analizaron la banda amida II (1450 cm^{-1}) comprendida por el modo de deformación N-H (1550 cm^{-1}) y las cadenas laterales y la banda amida II' comprendida por el modo de deformación N-D (1550 cm^{-1}) para determinar la interacción de las cadenas laterales y el grado de solvatación (80% para $^{13}\text{C-Cen}$, 100% para MLT y 100% $^{13}\text{C-}$

Cen/MLT). La interacción entre el complejo de proteínas, esta dominada por MLT, lo que es sugerido por los efectos observados en los motivos α -hélices de centrina a un mayor grado que su interacción con calcio. Este efecto se observó en los estudios de calorimetría en donde la pre-transición de centrina se desplazó en 13 °C, de 81 °C a 95 °C. Finalmente, estos resultados que apoyan para el estudio de otros péptido blancos de centrina para poder entender los cambios biofísicos y bioquímicos que conducen a su interacción.

Copyright © by
Liliana del Valle Sosa
2006

To my family . . .

ACKNOWLEDGEMENTS

I want to express my sincere acknowledgements to my advisor Dra. Belinda Pastrana-Ríos, for opportunity to do research under her guidance and supervision. Also, thanks to my graduate committee members, Dra. Doris Ramírez and Dr. Jorge Ríos Steiner.

My acknowledgements to the Department of Chemistry and its Director, Dra. María Aponte for providing me financial assistance during my master studies.

The NIH-SCORE Grant SO6GM08103 and Cobre II provided the funding and the resources for the development of this research.

Thanks to the international group and friends of Lab Q307 and Lab Q385: Daniel, Ibon, Zuleika, Myrna, Syndi, Jessica, Veronica, Ana María, Muriel and Christina for unconditional help and encouragement.

Finally, but the most important, my special thank to my parents, Rodolfo and Elva, for the attention, patience, best desires and the love given through the distance. To my brothers, Eduardo and Sergio, for their continuous support and help in every situation I need them.

TABLE OF CONTENTS

ABSTRACT	II
RESUMEN	IV
ACKNOWLEDGEMENTS	VIII
TABLE OF CONTENTS	IX
LIST OF TABLES	XII
LIST OF FIGURES	XIII
CHAPTER I	1
INTRODUCTION	1
1.1 Objectives	4
1.2 Summary of Following Chapters	4
CHAPTER II	5
PREVIOUS WORK	5
CHAPTER III	12
THEORETICAL BACKGROUND	12
3.1 General considerations	12
3.2 Attenuated total reflectance (ATR) FT-IR	20
3.3 Hydrogen/Deuterium exchange	21
3.4 Thermal unfolding and stability	22

3.5	Two-dimensional correlation analysis -----	24
CHAPTER IV -----		28
MATERIALS AND METHODS -----		28
4.1	Synthetic Melittin-----	28
4.2	¹³ C- <i>Chlamydomonas</i> centrin -----	28
4.2.1	Bacterial expression -----	28
4.2.2	Isolation and Purification of ¹³ C- <i>Chlamydomonas</i> centrin-----	29
4.3	FT-IR spectroscopy -----	30
4.3.1	H/D exchange analysis-----	30
4.3.2	Thermal Dependence Studies -----	31
4.3.3	Data analysis -----	32
4.4	Differential Scanning Calorimetry (DSC)-----	32
CHAPTER V -----		34
RESULTS AND DISCUSSIONS -----		34
5.1	Bacterial over-expression of ¹³ C- <i>Chlamydomonas</i> centrin-----	34
5.2	Isolation and Purification of ¹³ C- <i>Chlamydomonas</i> centrin-----	36
5.2.1	Phenyl Sepharose CL4B Chromatography -----	36
5.2.2	Anion Exchange Chromatography -----	38
5.3	Ultra Violet Spectroscopic analysis -----	40
5.4	Mass Spectrometry Analysis-----	41
5.5	FT-IR Spectroscopy -----	43
5.5.1	H→D Exchange Analysis -----	43
5.5.2	Kinetics of exchange -----	46
5.5.3	Two Dimensional Correlation Analysis (2D-COS) during the H/D exchange process -----	50
5.6	Thermal Dependence Studies -----	54
5.6.1	Two dimensional correlation analysis -----	58

5.6.2	Thermal Dependence Studies	64
5.7	Differential Scanning Calorimetry (DSC)	67
CHAPTER VI		69
CONCLUSIONS		69
6.1	Summary	69
6.2	Main conclusions	70
6.3	Future work	70
REFERENCES		72

LIST OF TABLES

	Page
Table 3.1-1 Characteristic infrared amide bands to study protein structure in aqueous solutions -----	16
Table 3.1-2 Typical band positions for characteristic amino acid side chains observed in the Mid-IR region of the spectrum -----	19
Table 5.5-1 2D-COS assignments of the synchronous and asynchronous plots for ¹³ C- <i>Chlamydomonas</i> centrin, melittin and ¹³ C- <i>Cen</i> /MLT complex. -----	52
Table 5.5-2 Summary of phase analysis used to determine H→D exchange dynamics in ¹³ C- <i>Chlamydomonas</i> centrin, melittin and ¹³ C- <i>Cen</i> /MLT complex. -----	53
Table 5.6-1 Summary of phase analysis used for thermal characterization in ¹³ C- <i>Chlamydomonas</i> centrin, melittin and ¹³ C- <i>Cen</i> /MLT complex. -----	62
Table 5.6-2 Summary of secondary structure assignment obtained from the synchronous and asynchronous plots for ¹³ C- <i>Chlamydomonas</i> centrin, melittin and ¹³ C- <i>Cen</i> /MLT complex. -----	63

LIST OF FIGURES

	Page
Figure 2.1 Scheme of the cell cycle -----	5
Figure 2.2 The nucleus-basal-body and flagella of <i>Chlamydomonas reinhardtii</i> -----	7
Figure 2.3 Structure predictions of <i>Chlamydomonas</i> centrin -----	8
Figure 2.4 Structure and sequence of melittin -----	10
Figure 2.5 A two component molecular thread model-----	11
Figure 3.1-1 N-methyl-acetamide structure -----	15
Figure 3.1-2 Amide I/I' frequencies summarized for protein secondary structure -----	18
Figure 3.2-1 Total internal reflection at the interface of an internal reflection element-----	21
Figure 3.5-1 General scheme for obtaining two dimensional correlation spectra-----	25
Figure 3.5-2 Schematic contour maps -----	26
Figure 5.1-1 Growth curve of transformed <i>E. coli</i> BL21- λ DE ₃ over-expression of ¹³ C- <i>Chlamydomonas</i> centrin -----	34
Figure 5.1-2 15% SDS-PAGE of ¹³ C- <i>Chlamydomonas</i> centrin expression-----	35
Figure 5.2-1 Phenyl sepharose chromatogram of purification of ¹³ C- <i>Chlamydomonas</i> centrin -----	36
Figure 5.2-2 15% SDS-PAGE analysis of eluted fractions from phenyl sepharose column--	37
Figure 5.2-3 Anion exchange chromatogram (0-0.75 M NaCl) of the purification of ¹³ C- <i>Chlamydomonas</i> centrin -----	38
Figure 5.2-4 15% SDS-PAGE analysis after anionic chromatography for the purification of ¹³ C- <i>Chlamydomonas</i> centrin-----	39
Figure 5.2-5 15% SDS-PAGE analysis of ¹³ C- <i>Chlamydomonas</i> centrin > 98 % pure -----	40
Figure 5.3-1 UV spectrum of ¹³ C- <i>Chlamydomonas</i> centrin. -----	41

Figure 5.4-1 TOF-ES mass spectrometer of ^{13}C - <i>Chlamydomonas</i> centrin. -----	42
Figure 5.5-1 Overlaid and difference spectra in the region 1700-1400 cm^{-1} -----	45
Figure 5.5-2 Single frequency kinetics of individual components and the complex -----	48
Figure 5.5-3 H→D exchange kinetics of ^{13}C - <i>Cen</i> , melittin and ^{13}C - <i>Cen</i> complex-----	49
Figure 5.5-4 Synchronous and asynchronous contours plots corresponding to ^{13}C - <i>Chlamydomonas</i> centrin (A,D), melittin (B,E) and ^{13}C - <i>Cen</i> /MLT complex (C,F) -----	50
Figure 5.6-1 Overlaid FT-IR spectra of (A) ^{13}C - <i>Cen</i> , (B) melittin and (C) ^{13}C - <i>Cen</i> / MLT complex -----	56
Figure 5.6-2 Overlaid FT-IR spectra of ^{13}C - <i>Chlamydomonas</i> centrin and ^{13}C - <i>Cen</i> / MLT complex at two calcium concentration -----	57
Figure 5.6-3 Synchronous and asynchronous contours plots corresponding to (A, D) ^{13}C - <i>Chlamydomonas</i> centrin, (B, E) melittin and (C,F) ^{13}C - <i>Cen</i> /MLT complex -----	61
Figure 5.6-4 Temperature dependence plots for ^{13}C - <i>Cen</i> and ^{13}C - <i>Cen</i> /MLT complex for two Ca^{+2} concentrations -----	65
Figure 5.6-5 Temperature dependence plot of MLT loops region in the complex-----	66
Figure 5.7-1 Thermograms of (A) ^{13}C - <i>Cen</i> , (B) melittin and (C) ^{13}C - <i>Cen</i> /MLT complex in the temperature range of 20 °C to 127 °C.-----	68

CHAPTER I

INTRODUCTION

To date, the Human Genome has been completed with a total of 33,000 genes (Venter et al., 2003). It is estimated, that the proteome should constitute at least 100,000 proteins. This disparity, between the number of genes and the proteome can be accounted by post-translational modifications and alternative splicing. Actually, the number of known protein structures remains small (about 26,000 proteins), according to the Protein Data Bank (PDB) (<http://www.rcsb.org/pdb>). In many cases, little is known about the structural basis for protein target recognition, important in understanding the signal transduction pathway.

Fourier transform infrared (FT-IR) spectroscopy has emerged in the last decade as a valuable technique to quantitatively determine secondary structure contributions in proteins. This is achieved by studying the contributions and underlying band area of the conformation-sensitive amide I band (Surewicz et al., 1993; Pastrana et al., 2002). In particular, this technique has shown great promise for the study of conformational changes in proteins (Ortiz et al., 2004, Pastrana et al., 2002, Casal et al., 1998, Prestrelski et al., 1991, Fabian et al., 1993). However, when different proteins are present in solution, their amide I bands overlap, making the interpretation ambiguous as with CD spectroscopy. It has been reported that carbon-13 isotope labeling in the carbonyl group causes a shift of the amide I band (essentially a C=O stretching vibration of the amide carbonyl groups) to lower frequencies (Jakson et al., 1989; Hübner et al., 1990; Pastrana-Rios et al., 2001). Hence by homogenously ¹³C-labeling a protein and adding an unlabeled protein or peptide, to generate

a complex, it is then feasible, to study both protein components within the complex simultaneously and studying their respective amide I' and amide I*' bands (the asterisk-prime is used to denote ^{13}C labeled protein) separately.

FT-IR spectroscopy is exquisitely sensitive to backbone conformation and can be used to study the extent of hydrogen/deuterium (H/D) exchange, as well as side chain interactions, particularly the aspartate (Asp^-), glutamate (Glu^-), arginine (Arg) residues (Pastrana et al., 2002, 2004). This technique is also well suited for the study of protein/peptide interactions that are sensitive to their environment. Additionally, FT-IR and DSC can be used to obtain the thermal transition temperature for each protein to establish their relative stability within the protein/peptide complex and the individual components.

In this work, we have used this strategy to analyze the interaction of ^{13}C -*Chlamydomonas* centrin (^{13}C -*Cen*), a low molecular weight, protein that belongs to the EF-hand superfamily of calcium binding proteins (Salisbury et al., 1989) with melittin (MLT), a 26 residue amphipathic peptide from bee venom, *Apis mellifera* (Weaver et al., 1989). MLT is known to exist in different structural forms depending on the protein conditions (Kampl et al., 1997). Centrin has been shown to interact with melittin in studies carried-out by Durussel and co-workers (2000) using fluorescence spectroscopy. Therefore, this complex would be an ideal system to study using FT-IR spectroscopy. Thermal dependence experiments of this protein/peptide complex would be ideal to determine relative thermal stability, dynamics, and conformational changes of the complex compared with the individual components.

MLT is an excellent choice as a model for oligomerization in that it lacks organized or stable secondary structure at sub-millimolar concentration in pure water, yet becomes predominantly helical and tetrameric when under high ionic strength or pH conditions

(Weaver et al., 1989). Melittin also serves as a useful model for the study of peptide-lipid interactions, since it interacts avidly with lipid surfaces, which is apparently a major factor in its ability to lyse lipid vesicles and cells (Kampl et al., 1997).

The uniqueness of this approach is to use FT-IR spectroscopy and two-dimensional correlation analyses (2D-COS) to study the dynamics of these proteins along with the secondary structural changes that may occur. We can compare the structural changes observed in centrin with a well-studied protein known as calmodulin. Both proteins have been shown to have a conformational change upon binding different target peptides, by using NMR spectroscopy and X-ray diffraction (Hu et al., 2004). Also, circular dichroism (CD) has traditionally been used to obtain percent secondary structure contributions in pure proteins (single component) and has been used to corroborate the overall conformational changes observed by FT-IR spectroscopy (Pastrana et al., 2000). The dynamic information obtained by FT-IR spectroscopy will be used to complement the information obtained by NMR and X-ray structure.

In summary, the ^{13}C -centrin/melittin experiments would provide a roadmap towards future centrin target protein studies with biological relevance such as centrosome duplication.

1.1 Objectives

The main objective of this thesis is to explore the level of protein/ peptide interaction using ^{13}C -*Chlamydomonas* centrin and melittin, a known interacting peptide. This interaction will be studied using FT-IR spectroscopy by measuring:

1. The extent of hydrogen/deuterium (H/D) exchange in the complex and the single component (^{13}C -*Cen* and MLT) to determine the extent of solvation.
2. The differences in transition of the complex and the single component in order to determine the relative stability.
3. Two-dimensional correlation (2D-COS) in order to analyse the dynamics of the protein complex and its interaction.

Additionally, differential scanning micro-calorimetry (DSC) studies will be performed to establish thermal transition temperature and stability in order to confirm the results obtained using FT-IR.

1.2 Summary of Following Chapters

Previous work and basic information related to the research presented in this thesis is introduced in Chapter 2. In Chapter 3 the necessary background and theory is developed. In Chapter 4, a description of materials and methods used in this work is provided. Obtained results and their interpretation are presented in Chapter 5. Finally, general conclusions and future work are presented in Chapter 6.

CHAPTER II

PREVIOUS WORK

Usually, when cells reach a certain size, they must either stop growing or divide. Some cells, such as nerve, skeletal muscle, and red blood cells, usually do not divide once they are mature. The activities of growing and dividing cells can be described in terms of the cell cycle. In cells capable of dividing, the cell cycle is the period from the beginning of one division to the beginning of the next, usually represented in diagrams as a circle (Figure 2.1). The time it takes to complete one cell cycle is the generation time. This can vary widely, but in actively growing plant and animal cells it is often about 8 to 20 hours (Salomon et al., 2003), within this time span, cell division averages 0.9 hrs a very small fraction of the time within the cell cycle. Typically only 3% of the cells undergo cell division at any given time.

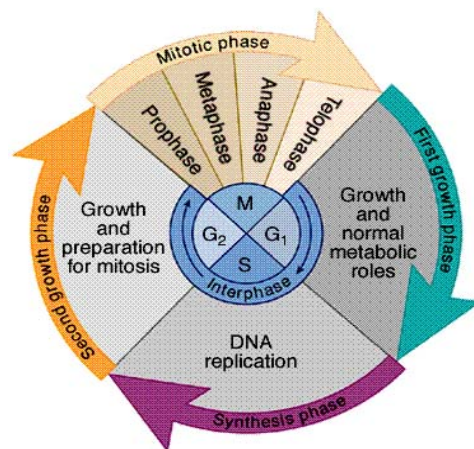


Figure 2.1 Scheme of the cell cycle. Describing the different phases including the mitotic phase. (Solomon, Berg, and Martin. Biology, 5th edition).

Cell division involves two main processes, mitosis and cytokinesis (Solomon et al., 2002). Mitosis is a complex process involving the nucleus, ensuring that each new nucleus receives the same number and types of chromosomes as were present in the original nucleus. Cytokinesis, which generally begins before mitosis is complete, changes the cellular membrane which leads to membrane fusion and separation of the cytoplasm. This process leads to the generation of two daughter cells. Multinucleated cells are formed, if mitosis is not followed by cytokinesis.

The inter-phase is the stage between successive cell divisions. Most of the life of the cell is spent in this phase. The cell is very active during this time, synthesizing needed proteins and growing.

It is estimated, that a hundred proteins are involved in cell division yet; only a few proteins have been characterized to date. The difficulty lies in their overall abundance and the time in which they are present in a functional form during the cell cycle, particularly during the mitotic phase (Salomon et al., 2002). Centrin is a ubiquitous protein component of the mitotic spindle pole, centrioles, and the centrosome. Genetic studies show that centrin is essential to the cell cycle-dependent duplication and segregation of the microtubule-organization center (MTOC). The microtubule-based cytoskeleton in eukaryotic cells is regulated by the MTOC, which organizes the number, direction, and polarity of the microtubules.

Since the discovery of centrin in the green alga *Tetraselmis striata*, homologue of the protein were identified in a wide variety of organisms ranging from protozoa and yeast to plants and humans (Salisbury et al., 1989, 1995). In *Chlamydomonas reinhardtii*, centrin-

based fiber contraction also plays a fundamental role in microtubule severing at the time of flagellar excision (Salisbury et al., 1995), (Fig. 2.2).

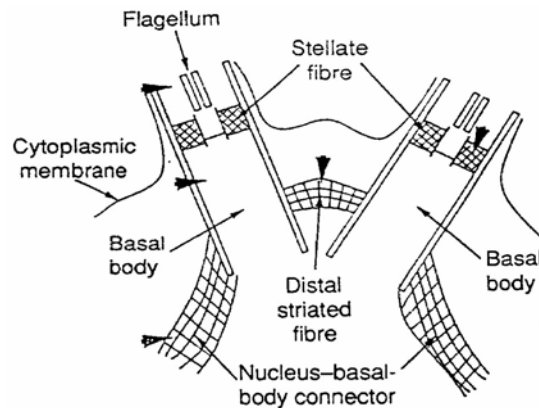


Figure 2.2 The nucleus-basal-body and flagella of *Chlamydomonas reinhardtii*. The arrow heads indicate the location of centrin in *Chlamydomonas* (Schiebel E. and Bornerns M., 1995)

Centrin is closely related to the EF-hand calcium sensor protein calmodulin (CaM), which also plays a role in centrosome function. Centrin and calmodulin share about 50% sequence identity (Fig. 2.3A). Both proteins are comprised of two structurally independent globular domains connected by a flexible linker, each domain containing two helix-loop-helix calcium binding motifs (Fig. 2.3B).

However, centrin is clearly distinguished from CaM by several characteristics. First, there are roughly 40 conserved residues in centrin that are not shared by calmodulin. Second, centrin contains a highly conserved positively charged amino terminal sequence of variable length that is absent in calmodulin. Third, a feature unique to centrin is the presence of a conserved aromatic residue (Tyr or Phe) at the carboxyl terminus, (Pastrana et al., 2002, 2004). Finally, centrin has distinct calcium binding properties with one or more calcium-

binding sites having significantly lower affinity than that observed in typical calcium sensors such as CaM.

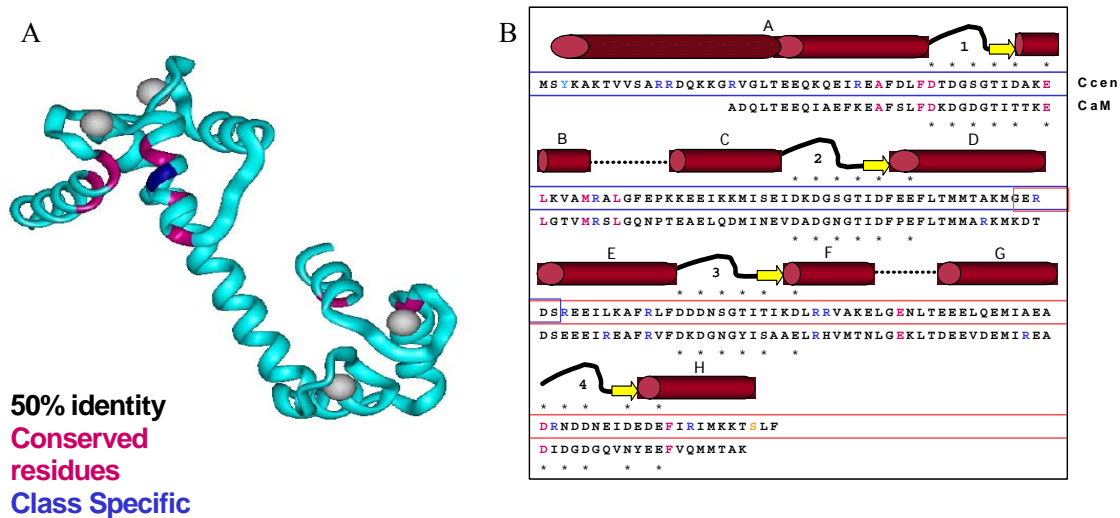


Figure 2.3 Structure predictions of *Chlamydomonas centrin*. (A) Structural homology for calmodulin, troponin C and centrin. (B) Sequence alignment of Ccen and Human calmodulin along with a schematic representation of CaM structural motifs. The red striped helix is the proposed secondary structure for the Ccen amino terminal end. Residues Arg (blue) and Tyr (cyan) are shown within each sequence, and in purple the conserved residues. The asterisk depicts the Ca^{2+} coordination site for the canonical and non-canonical binding site. The terminal domain fragments Ccen-N and Ccen-C sequence shown have been boxed in blue and red, respectively (Ortiz et al., 2004).

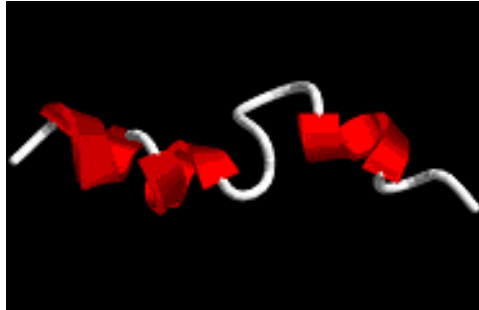
Experimental methods, such as Fluorescence (Durussel et al., 2000) circular dichroism (Perczel et al., 1992), attenuated total reflectance (ATR) FT-IR (Raussens et al., 2004, Ortiz et al., 2004), and NMR spectroscopy (Weaver et al., 1992, Hu et al., 2004), among others, have been used to examine structure, dynamics, and relative stability of centrin and centrin/peptide complexes. All of these methods provide information about protein or peptide secondary structure and/or their environment.

In 2001, Pastrana et al. studied the mechanism of unfolding of a model helical peptide using FT-IR spectroscopy and two-dimensional correlation analysis. They demonstrated the usefulness of FT-IR 2D-COS analysis to simultaneously study amide I' and amide I'* bands ($^{13}\text{C}=\text{O}$ labeled peptide carbonyls of certain alanine residues) along with contributing side-chain modes for peptide unfolding.

Cox and collaborators (2000) report the Ca^{+2} binding characteristic of human centrin 2, as well as the effect of Ca^{+2} on conformation of this protein and its interaction with melittin. They find that the affinity of centrin 2 is 30 times less, than that of the calmodulin for melittin. These results suggest that the mode of target activation by centrin 2 is very different from the well-established model for calmodulin. Similar results were obtained for human centrin 3/melittin complex (Craescu et al., 2005).

Calmodulin has been studied extensively and is known to serve as a sensor for intracellular Ca^{+2} signals. It functions *via* Ca^{+2} -dependent interactions with many known cellular targets and is involved in regulating a wide range of cellular processes (Comte et al., 1983). The structural basis for Ca^{+2} -induced target activation by CaM and related EF-hand superfamily proteins has been established by comparing their NMR and X-ray structures in the absence and in the presence of calcium. For CaM, it has been shown that Ca^{+2} -induced conformational changes within each EF-hand domain leads to the exposure of hydrophobic surfaces along with secondary structural changes resulting in a wrap around conformation (Hu et al., 2003). The structures of more than a dozen $(\text{Ca}^{+2})_4$ -CaM complexes with small peptide fragments from known targets directly demonstrated the binding of targets within these hydrophobic cavities (Maulet et al., 1983, Cox et al., 1985).

Moreover, calmodulin has been shown to form exceptionally tight, calcium-dependent complexes with several natural peptides such as melittin (structure and sequence shown in Fig. 2.4) and RS20 (Fisher et al., 1994). These peptides were demonstrated to be capable of forming basic, amphipathic α -helices.



GIGAILKVLA TGLPTLISWI KNKRKQ

Figure 2.4 Structure and sequence of melittin. α -helices (red) and in loops structures (white).

To further illustrate the importance of this structural feature for calmodulin binding, several other amphipathic α -helical peptides were tested for their ability to bind calmodulin. Complex formation between calmodulin and a 14-residue basic peptide leads to an increase in the helicity (50%) within the complex which is attributed to an increase in the helicity of the peptide. Calmodulin also interacts with the neutral α -helical peptide toxin delta-hemolysin. Upon binding of the peptide, a fluorescence emission of a 2-fold increase was observed along with a blue shift of the fluorescence maximum. Resulting in a dissociation constant that could not be unambiguously estimated, due to delta-hemolysin tendency to self-associate (Cox et al., 1985)

Chazin et al., 2003, reported a comparison between centrin C-terminal domain fragment Ccen-C/Kar1p complex and CaM/Kar1p complex. This comparison revealed the

structural basis for target specificity and described the first high resolution structure of a centrin/peptide complex. Other studies carried-out by this group, contributed to the determination of Ccen-C conditional binding to Kar1p in a calcium dependent manner, while the N-terminal domain (Ccen-N) does not show any appreciable affinity for Kar1p, (Chazin et al., 2004).

In a recent study combining yeast genetics, genome databases mining and clever cell biology, Kilmartin (2003) has identified a novel centrosome protein, Sfi1, with a striking series of internal centrin-binding repeats. He carried-out a pull-down experiment in which a recombinant-tagged version of a centrin homologue in yeast known as Cdc31 was used to identify centrin binding partners. In addition, Salisbury (2004) proposed a model in which Sfi1 serves as a flexible elastic fiber along which multiple centrin molecules are tightly bound at low calcium concentrations. When free Ca^{2+} increases, the centrin molecule binds Ca^{2+} ions and undergoes a conformational change resulting in torsional forces along the length of Sfi1 causing bends or twist consequently shortening its overall length (Fig. 2.5).

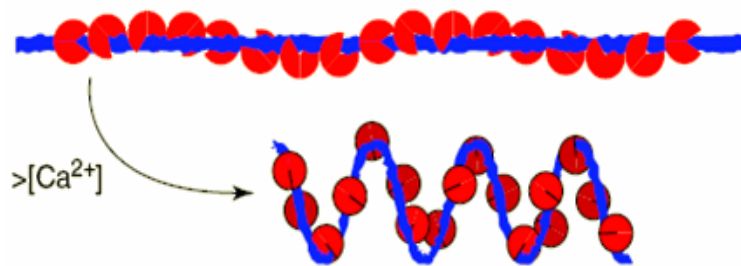


Figure 2.5 A two component molecular thread model. Sfi1 (blue rod) is containing 23 binding sites for centrin (red). Upon calcium influx contraction of Sfi1 protein is proposed (Salisbury, 2004).

CHAPTER III

THEORETICAL BACKGROUND

3.1 General considerations

There are different ways to predict protein secondary and tertiary structure. One commonly used method is homology based on sequence of known domains with putative function within the same protein class (Pearl et al., 2005). A second method uses the physical chemical properties of the amino acid sequence comprised in a protein (Yang, 1996).

In an effort to resolve the protein structure many techniques have been applied. Electron microscopy (EM) has been implemented towards determining the surface structure (tertiary structure) of protein complexes and membrane proteins (Stahlberg, 2002). The results obtained are of high quality, high resolution images of proteins in the native state, allowing a critical inspection of the surface contour of a protein and determination of the existence of an aggregated state. EM is also used to determine purity of a protein sample. In addition, this technique is particularly advantageous for membrane protein preparations where detergent micelles are used.

There are several spectroscopic techniques commonly used such as X-ray diffraction crystallography, and nuclear magnetic resonance (NMR) which are high resolution techniques. Other techniques like neutron scattering (Gabel et al., 2002), resonance Raman (Tracewell et al., 2005), circular dichroism (CD) (Perczel et al., 1992), and Fourier transformed infrared (FT-IR) (Pastrana-Rios et al., 2002, Arrondo et al., 1999) spectroscopies, are low resolution techniques. Within infrared techniques there are a number

of alternatives known as: coherent two-dimensional infrared spectroscopy (2D-IR) (Xu et al., 2003), phase modulated infrared reflection absorbance spectroscopy (PM-IRRAS) (Lavoie et al., 2002), infrared reflection absorption spectroscopy (IRRAS) (Pastrana-Rios et al., 1995, Shanmukh et al., 2005), transmission infrared (Pastrana-Rios et al., 2000), and attenuated total reflectance (ATR) (Ortiz et al., 2004) spectroscopy. These techniques are used to determine percent of secondary structure, changes in conformations, and side chain interactions (H-bonding, salt bridging and/or ionic interactions).

X-ray diffraction crystallography is the method chooses for detailed protein structure analysis and three dimensional studies. However, obtaining high quality crystals of proteins is not easy (Creighton, 1993) and for that reason number of different proteins that have been crystallized has not increased significantly.

Multi-dimensional nuclear magnetic resonance (NMR) is also a rapidly progressing method for the structure determination of biological macromolecules in aqueous solution. However, this method is limited to macromolecules with masses below 60 kDa (protein of lower molecular weight) and large protein concentrations are required to determine the solution structure of the protein. In spite of these conditions, Wutrich in 2005, resolved the structure of a protein complex such as GroEL (60 kDa) and developed a methodology for NMR experiments that resolve the dynamics of proteins.

Due to these limitations, it is possible to choose a technique with low resolution that complements other techniques. In many aspects of protein structure/function relationship determination by lower resolution techniques have been used even in proteins with known three-dimensional structure.

FT-IR spectroscopy has been experienced an increase of applications that provide molecular information in systems that range from the level of amino acid, small peptides, isolated proteins, enzymes and lipids to even more complex systems such as protein/peptide, and lipid/protein interactions (Arrondo et al., 1999, Ortiz et al., 2004, Pastrana et al., 2002, Raussenns et al., 2004). This technique probes molecular vibrations in molecules providing secondary structure information and side chain interactions. The structural information obtained is dynamic and can also be in the micro-second time scale by applying time-resolved FT-IR spectroscopy (Ortiz et al., 2004, Raussenns et al., 2004).

An important advantage of FT-IR spectroscopy is that the size of a protein or the nature of the environment, does not limit its application. Proteins with molecular weight of up to 200 kDa or more can be studied (Fabian et al., 2002). Furthermore, sample quantities can be reduced from milligrams to micrograms, which make this technique a lot more attractive for biochemical and biological studies.

On the other hand, measurements can be performed in aqueous solutions or organic solvents, in oriented films or deposits, as well as in detergents or membrane-like environments (Fabian et al., 2002).

Infrared spectroscopy was first applied to proteins, as early as 1952 (Sutherland, 1952) before any detailed X-ray structure was available for proteins. These studies demonstrated that a strong correlation between vibrational frequency (band position) and the predominant structure of synthetic homo-polypeptides in aqueous solutions. The amide group that forms the peptide bond is the most abundant functional group found in a protein. In order to characterize vibrational modes of the amide group, also termed amide I band, of N-methylacetamide (Fig. 3.1-1) a simple molecule was studied (Krimm, 1986).

Later, these experimental observations were refined by making detailed vibrational analyses of the structure of the amide I band in order to establish a correlation between the frequencies of these bands and the corresponding secondary structure, such as purely α -helical or purely β -sheet structures. Thus, nine amide bands were established within the mid-IR spectral region (Table 3.1-1).

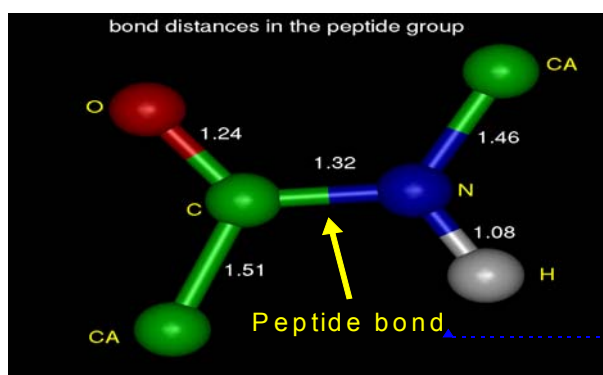


Figure 3.1-1 N-methyl-acetamide structure.

Table 3.1-1 Characteristic infrared amide bands to study protein structure in aqueous solutions. (Fabian H. and Mäntele W., 2002)

Nomenclature (amide)	Vibrational modes	Approximate frequency (cm ⁻¹)
A	NH stretching in resonance with 1st	~ 3300
B	amide II overtone	~ 3100
I	CO stretching	1610-1695
II	NH bending and CN stretching	1480-1575
III	CN bending and NH stretching	1220-1320
IV	OCN bending, mixed with other modes	625-765
V	Out-of-plane NH bending	640-800
VI	Out-of-plane CO bending	535-605
VII	Skeletal torsion	~ 200

Of all the amide bands described in the table above, the most intense and most useful for the analysis of secondary structure in proteins was found to be the amide I band. The amide I band is comprised primarily of C=O stretching vibrations of the peptide bond (though coupled to in-plane bending of the N-H and stretching of the C-N bond) within the spectral region of 1600-1700 cm⁻¹.

Infrared spectroscopic studies of proteins in water are complicated by the fact that the H-O-H bending vibrations of H₂O absorb very strongly at 1640 cm⁻¹. As a consequence, very short pathlengths 3-8 μm are needed for transmission measurements in the amide I region (1700-1600 cm⁻¹) to prevent water absorption interference. In addition, the amide II

region (1600-1500 cm^{-1}) is completely overlapped by this H-O-H association band. Therefore, no information about the side chains can be extracted (Fabian et al., 2002).

However, experimentally protein spectra can be obtained in deuterium oxide (D_2O) solutions with a pathlength of 40 μm . The infrared bands of D_2O occur at a lower wavenumber region (2500-2000 cm^{-1}), allowing for the studies of the amide I and amide II bands associated with proteins.

Consequently, the protein secondary structure can be determined by analyzing the amide I/I' bands due to their sensitivity to hydrogen bonding pattern, dipole-dipole interaction and the geometry of the protein backbone. Usually, the amide I/I' band of proteins consist of a series of overlapping contributions (α -helices, β -sheets, turns and unordered structures) which occur as a results of the secondary structures present in the protein of interest (Fig. 3.1-2).

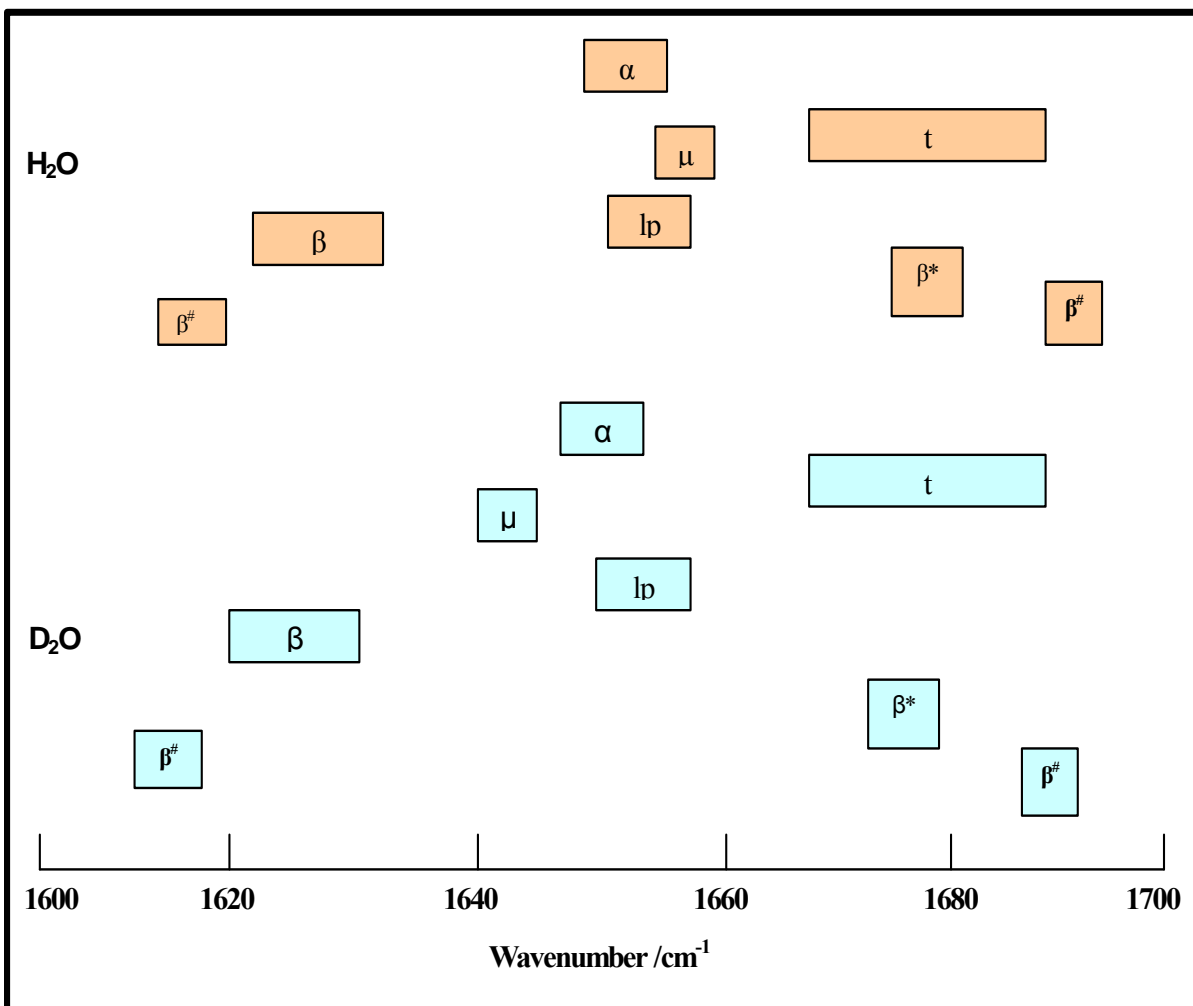



Figure 3.1-2 Amide I/I' frequencies summarized for protein secondary structure. The amide I contributions in H₂O (orange box) and amide I' band contributions in D₂O (light blue) are shown. α : α -helices. In highly solvent-exposed α -helices the amide I' band can shift to 1630-1645 cm⁻¹ due to additional hydrogen bonding of the solvent accessible C=O groups to water. β : β -sheet structures, for proteins often more than one more component is observed. This reflects differences in hydrogen bonding (the stronger and shorter the hydrogen bond, the lower frequency) as well as differences in transition dipole coupling in different β -strand. $\beta^\#$: β -strands in aggregates. IR spectra of thermally aggregated proteins are characterized by a significant increased in splitting between the low and high frequency β -components (β and β^* , respectively) in comparison to that observed from the β -sheet in native proteins. μ , unordered parts of the polypeptide backbone; lp, loops; t, turns (Fabian and Mäntele, 2002).

On the other hand, some side chains absorb in the amide I/I' or amide II region (Table 3.1-2), but the contribution of the amino acid side chains depends on their protonation state. However, the spectral features of the side chain absorption bands can be used to study weak interactions in the proteins.

Table 3.1-2 Typical band positions for characteristic amino acid side chains observed in the Mid-IR region of the spectrum (Chirgaze, 1975 and Graff et al., 1997).

Amino acid (side chain)	R group	Wavenumber/ cm^{-1}
Asp ⁻	-CH ₂ COO ⁻	1585
Glu ⁻	-(CH ₂) ₂ COO ⁻	1570
Arg ⁺	-(CH ₂) ₃ NHCNH ₂ NH ₂ ⁺	1605 (s), 1586 (a)
Tyr	-CH ₂ --  -OH	1515

FT-IR spectroscopy permits a detailed analysis of variant proteins and its effect of point mutations in the secondary structure or substrate binding. Relative stability can also be accessed by comparing wild-type and variant proteins.

Also, isotope labeling, such as site-specific ¹³C-labeling of the protein backbone, allows for location of a particular secondary structure within the protein chain and helps in analyzing conformational changes from the labeled site (Pastrana-Ríos et al., 2001).

3.2 Attenuated total reflectance (ATR) FT-IR

The increased sensitivity of modern infrared spectrometers has also allowed for the use of sampling techniques other than transmission. Reflection techniques, and particularly attenuated total reflectance (ATR), have been applied to study protein secondary structure, solvent accessibility and orientation of anisotropic samples (Raussen et al., 2004). This technique yields a strong signal with only a few micrograms of sample (100-1000 μg) and spectra are recorded in a few minutes. The environment of the molecules can be modulated so that their conformation can be studied as a function of temperature, pressure, pH, isotope exchange, as well as the titration of specific ligands.

For ATR measurements, the sample (dry or solution) is applied onto a surface of a trapezoidal-shaped IR-transparent crystal, e.g., zinc selenide (ZnSe) or germanium (Ge). IR radiation is focused onto the end of the crystal and multiple internal reflection elements (IRE) occur. At each internal reflection, the IR radiation actually penetrates a short distance ($\sim 1 \mu\text{m}$) from the surface of the IRE into the interphase medium (Fig 3.2-1). It is this unique physical phenomenon (evanescent wave) that enables one to obtain infrared spectra of samples placed in contact with the IRE.

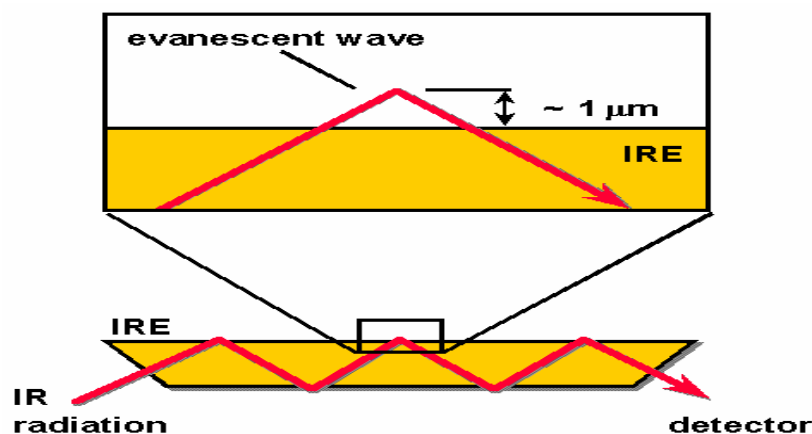


Figure 3.2-1 Total internal reflection at the interface of an internal reflection element (<http://www.micromenanalytical.com>).

3.3 Hydrogen/Deuterium exchange

ATR-FT-IR has been proven successful in the study of H→D exchange process in proteins. Furthermore, a particularity of infrared spectroscopy is that it allows monitoring the exchange rate of the amide protons, yielding data directly proportional to the number of amino acid residues in the protein. This technique is also used to study exchangeable side chains protons, i.e. -NH, -OH and -SH, which have identifiable exchange rates that depend on the global and local accessibility of the group and on its pKa value (Fabian et al., 2002).

This process has been shown to be extremely sensitive to environmental changes without perturbing the protein secondary structure. In addition, the kinetics of the exchange process can be determined (Ortiz et al., 2004). It is a useful technique to identify solvent accessible domains by identifying fast exchanging protons at the protein surface; somewhat slower exchanging protons correspond to the regions buried within the protein.

The spectral changes involved the amide I→I' with a slight shift of 10 cm^{-1} , while a concomitant decrease in intensity of amide II band (predominantly of the N-H bending, coupled with C-N stretching modes, and side chains) at 1550 cm^{-1} , and an intensity increase of the amide II' band at 1450 cm^{-1} during exchange (H→D). The relative intensities of the amide II and the amide II' bands of a protein in D_2O can be used to monitor the time course of the extent of hydrogen-deuterium exchange, and provide valuable information on the flexibility, dynamics and kinetics of exchange process.

3.4 Thermal unfolding and stability

Another application of FT-IR spectroscopy is transmission spectroscopy which is used to characterize protein thermal denaturation. The protein solution is applied to a window and placed in a thermostated cell jacket inside the sample chamber of the spectrophotometer and the temperature can be changed in a stepwise or continuous manner.

Calcium fluoride (CaF_2) windows are commonly used because (i) it has a low refractive index which is similar to that of water, (ii) its solubility index is low when compared to other materials, and (iii) it is transparent within the mid-infrared ($>1000\text{ cm}^{-1}$) of the spectrum. Moreover, for measurements at high temperatures and/or for long time periods, the sealing surface of the disks can be covered with mineral oil/ CHCl_3 mixture. This prevents both evaporation of the solvent (e.g. water) at high temperatures (e.g. 95°C), or changes in the isotope content when working with D_2O solution.

There are different ways to analyze the spectral data obtained. For the desired protein, a usual method is to construct intensity *vs.* temperature or wavenumber *vs.* temperature profiles for selected infrared bands.

Another approach used for the quantitative estimation of protein secondary structure involves the curve fitting of the amide I/I' band (1700-1550 cm^{-1}). The percentages of different secondary structures comprised in the protein studies are then estimated by adding the areas of all component bands assigned to each of these structures and expressing the sum as a fraction of the total amide I/I' band area (Arrondo et al., 1999, Fabian et al., 2002). This curve fitting approach has some significant inherent problems. An element of subjectivity is the assumption that the number of the component bands (sub-bands) estimated is accountable for the experimental spectrum. However, self deconvolution and second derivative spectra are commonly used to determine the real number of the components that contribute to the experimental spectra. In cases where bands are significantly overlapped, even the applied band narrowing procedures will certainly fail to separate the components present. This is especially critical in cases in which these components describe different types of secondary structures. One solution is to use the auto peaks obtained from 2D-COS analysis to define the number and position of the sub-bands, in this way eliminating the subjectivity associated with the curve fitting analysis.

3.5 Two-dimensional correlation analysis

Two-dimensional correlation spectroscopy (2D-COS) is a new technique implemented by Isao Noda in 1998. It has been established as a viable means to analyze and extract useful information from conventional one-dimensional spectral data and it has been considerably and successfully applied to a variety of spectroscopic techniques (IR, NIR, Raman, visible, fluorescence). This technique requires an external perturbation i.e. thermal, mechanical, chemical, spatial position, etc; and is employed for the enhancement of overlapping bands in the spectral region of interest.

In a correlation experiment, an external perturbation is applied to the sample and the infrared radiation is used as a probe. The external perturbation can be any perturbation that modifies the spectrum, sometimes called dynamic spectra. The effect of perturbation induces changes in local molecular environment and will be manifested by time-dependent fluctuations of various spectra representing the system. Correlation analysis of the spectral fluctuations leads to two-dimensional maps that increase the spectral resolution by spreading peaks along a second dimension, revealing the number of peaks perturbed, their maxima and the order of events as well as their correlations due to the perturbation applied (Fig. 3.5-1).

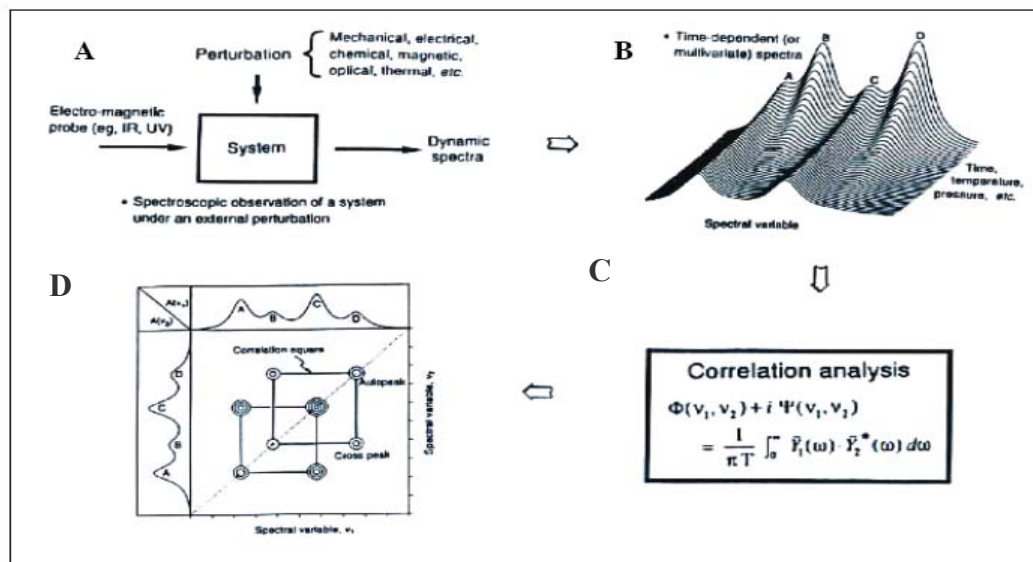


Figure 3.5-1 General scheme for obtaining two dimensional correlation spectra. A) Generation of contour plots are based on the the dynamics spectra, B) Dynamic spectrum generated, C) General equation of correlation analysis, and D) Two-dimensional spectrum obtained (synchronous spectrum) (Noda I., 2000).

Two types of spectral representations are obtained: synchronous and asynchronous plots. The synchronous plot is comprised of in phase intensity changes, whereas the asynchronous plot is has out of phase intensity changes. The synchronous plot is characterized by auto-peaks located on the diagonal and by cross peaks that are located off diagonal. Auto-peaks are observed when spectral features vary as a function of the applied perturbation (always positive). Cross-peaks can either be positive or negative. They reflect correlated changes that occur in phase or out of phase (Fig. 3.5-2A).

On the other hand, the asynchronous plot is characterized by having cross-peaks with positive and negative intensities. Asynchronous spectra are of particular interest, because they allow one to distinguish spectral intensities that vary slightly out plane, and thus, allow for the determination of the order of events (Fig. 3.5-2B).

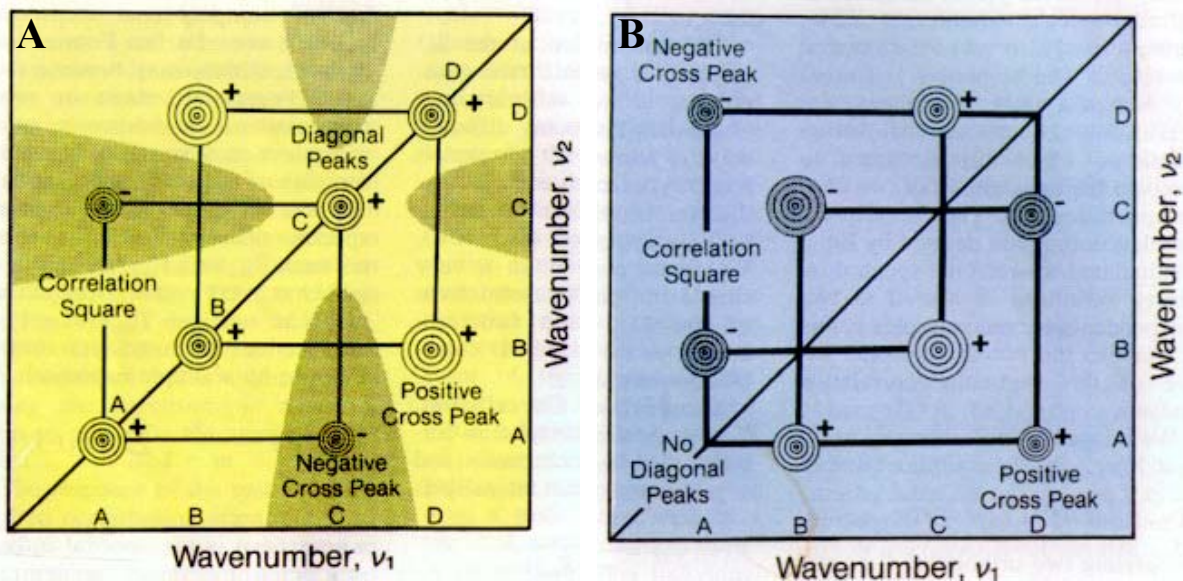


Figure 3.5-2 Schematic contour maps. Synchronous (A) and asynchronous (B) two dimensional correlation spectrum (Noda I., 2000).

A simple set of rules are used to determine the temporal sequence of events (Fig. 3.5-2). For cross peaks located at an arbitrary coordinate (ν_1, ν_2) of an asynchronous 2D-COS spectrum (Noda, I., 1990), the following rules are:

Rule 1: if the asynchronous cross-peaks is located at the upper left section of the spectrum ($\nu_1 > \nu_2$), and the sign of the peak is positive, the dipole-transition moment associated with the band at the higher wavenumber ν_1 reorients before the transitions moment at ν_2 .

Rule 2: if the positive asynchronous cross-peak is located at the lower right section of the spectrum ($\nu_1 < \nu_2$), the dipole-transition moment at lower wavenumber ν_1 reorients before the transition moment.

Rule 3: for a negative cross peak, the temporal relationships described in Rules 1 and 2 are reversed.

Rule 4: if the corresponding synchronous correlation intensity at the same coordinate is negative, the temporal relationship described in rules 1, 2 and 3 are reversed.

Rule 5: if the asynchronous correlation intensity at the coordinated vanished, the reorientations of the two dipole-transitions occur simultaneously.

Rule 6: if the synchronous correlation intensity at the same coordinate vanished, the temporal relationship between the reorientations of dipole-transition moment cannot be determined.

The ability of the 2D-COS analysis to enhance spectral resolution and determine the sequence of events in response to external factors is very attractive for the study of thermal denaturation (unfolding event). This technique could also be applied to studies focused on ligand binding, protein–protein or protein-lipid interactions which may affect protein-domain stabilization. In combination with isotope labeling, two-dimensional correlation analysis offers possibilities to identify individual unfolding events in a protein complex and establish the order of events leading to thermal denaturation.

CHAPTER IV

MATERIALS AND METHODS

4.1 Synthetic Melittin

Synthetic melittin (MLT) peptide was generously supplied by Dr. Frank Prendergast from Mayo Clinic and Foundation in Rochester, Minnesota. The peptide was dialyzed against 0.1 M HCl and freeze dried to remove residual trifluoroacetic acid (TFA). The lyophilized peptide sample was then re-solubilized in the appropriate buffer for its biophysical characterization.

4.2 ^{13}C -*Chlamydomonas centrin*

4.2.1 Bacterial expression

Chlamydomonas centrin was over-expressed using a pT 7-5 plasmid construction and *E. coli* BL21- λ DE₃. Bacterial cells were grown in 5.0 L of MARTEk 9 (Columbia, MD) minimal media (>98% ^{13}C atom) and 50 $\mu\text{g}/\text{mL}$ of ampicillin, using Bioflo 3000 fermentor from New Brunswick Scientific (Edison, NJ). The bacterial cells were incubated at 37°C, pH 7.00, and dissolved oxygen (DO_2) was set to 100%. Cell growth was monitored *via* optical density (OD) measurements at 550 nm. Protein expression was induced with 0.5 mM isopropyl- β -D-thiogalactopyranoside (IPTG) when cells have entered *log* phase. Three hours after induction, the cells were harvested and frozen for purification at a later time.

4.2.2 Isolation and Purification of ¹³C-*Chlamydomonas* centrin

Frozen cells were thawed in a lysis buffer (50 mM Hepes, 0.5 mM EDTA, 0.5 M NaCl, 0.1% Igepal, 0.04 % NaN₃) containing a cocktail of protease inhibitors (20 mg/ml Aprotinin, 0.5 mg/ml Leupeptin, 1.0 mg/ml Pepstatin) and sonicated with a macro probe 3 x pulse at 60 pulse/sec with 1 min rest periods while on ice. The lysate was centrifuged at 10,000 rpm for 15 min at 4°C. The supernatant was recovered and adjusted to 2 mM CaCl₂ and 4 mM MgCl₂ followed by a second centrifugation step at 31,000 rpm for 30 min at 4°C. The supernatant obtained on the last centrifugation was then filtered using a low protein affinity PES membrane with a 2 µm pore size.

The filtered supernatant was applied to a Phenyl Sepharose CL-4B column. This affinity column was equilibrated with a buffer containing solution of 50 mM Tris, 0.5 mM EDTA, 0.5 M NaCl, 4.0 mM MgCl₂, 4.0 mM CaCl₂, 0.1% IGEPAL, and 0.04% NaN₃. ¹³C-*Chlamydomonas* centrin eluted with an elution buffer that contained 50 mM Tris, 0.5mM EDTA, 5.0 mM EGTA, 0.5 M NaCl, 4.0 mM MgCl₂, 4.0 mM CaCl₂, and 0.04% NaN₃. Fractions containing centrin were identified *via* 15% Sodium dodecyl (lauryl) sulfate-polyacrylamide gel electrophoresis (SDS-PAGE). Fractions positive for centrin were pooled, concentrated, and re-equilibrated using a Millipore ultrafree membrane (5,000 MW cut off) in a different buffer solution containing 20 mM Hepes, 1 mM CaCl₂, 1 mM DTT at pH 7.4 and subjected to a second chromatographic step using a strong anion-exchange column. The elution was done with a NaCl gradient (0 to 0.75M), fractions were collected, and aliquots from every fraction were analyzed with at 15% SDS-PAGE.

Fractions containing centrin were pooled for UV spectral analysis and electron-spray-time-of-flight mass spectrometry (ES-TOF-MS). These steps were carried-out to determine the purity, molecular weight and integrity of ^{13}C -*Chlamydomonas* centrin (mass spectrometry analysis was carried-out at the Mayo Clinic and Foundation, Protein Core Facility).

The purified recombinant protein was concentrated using Millipore ultrafree membrane (5,000 MW cut off) in the following buffer, containing 50 mM Hepes, 150 mM NaCl, 4 mM CaCl_2 , 4 mM MgCl_2 , lyophilized, and stored at $-20\text{ }^\circ\text{C}$.

^{13}C -*Chlamydomonas* centrin's concentration was determined by direct UV absorbance at 274 nm after turbidity correction using ORIGIN 7 program. The calculated molar extinction coefficient used was $1309.9\text{ M}^{-1}\text{ cm}^{-1}$ in presence of cations.

4.3 FT-IR spectroscopy

4.3.1 H/D exchange analysis

The purified sample preparation was dialyzed against 16 mM Hepes, 50 mM NaCl, 2 mM CaCl_2 , 2 mM MgCl_2 , at pH 7.4 using a dialysis membrane (Centricon Centrifugal Filter Devices, Amicon) with a MW cutoff of 10,000 for ^{13}C -*Cen*. Melittin was dissolved in the same buffer.

Typically, 0.5-1 mg of ^{13}C -*Cen*, melittin or ^{13}C -*Cen*/MLT complex were used for the studies. The protein solution was spread on a hydrophilic germanium (Ge) surface of an attenuated total reflectance (ATR) crystal. The sample was purged with dry air, until a dry film was obtained. Spectra were recorded relative to a clean crystal at room temperature ($\approx 20^\circ\text{C}$) using a Mattson Infinity Series FT-IR Spectrophotometer equipped with an

horizontal ATR accessory comprised of a 45° angle of incidence Ge crystal with a mercury-cadmium-telluride (MCT) detector. Spectral data was obtained by acquiring 64 scans, during every one minute, for the first 20 minutes. Followed by subsequent data acquisition of 512 scans every 10 minutes at a resolution of 4.0 cm⁻¹ and data encoded every 2 cm⁻¹. A representative spectrum of the fully proteated sample was collected. The sample film was then hydrated with a flow of D₂O vapor for 6 hours approximately or until no significant exchange was observed.

4.3.2 Thermal Dependence Studies

4.3.2.1 Sample preparation

A total of 0.42 mM of each ¹³C-*Cen*, melittin or ¹³C-*Cen*/MLT complex (1:1, mol:mol) was repeatedly lyophilized and re-suspended in 50 μL containing 50 mM Hepes, 4 mM CaCl₂, 4 mM MgCl₂, and 150 mM NaCl at a pD 6.6 in D₂O (99% atom D) until complete hydrogen→deuterium (H→D) exchange had occurred.

The protein sample was placed between two circular custom-milled calcium fluoride (CaF₂) windows (50 x 4 mm) with a 40 μm path-length from Spectral System, LLC and sealed with 25 μl of chloroform/mineral oil mixture for a proper seal. The reference cell was prepared similarly using 30 μL of isotonic D₂O. The sample and reference cells were inserted in a custom dual chamber thermostated cell holder. The temperature within the cell was controlled using Neslab RTE-740 Refrigerated circulating bath from Thermo Electron Corp. (Madison, Wisconsin), and monitored with a thermocouple sensor from Physitemp Model Bat-12 (Clifton, NJ) positioned in close contact to the sample window assembly.

4.3.2.2 Thermal perturbation studies

Background and sample spectra were acquired using a Nicolet Magna-IR 550 FT-IR spectrometer equipped with a deuterated triglycine sulfate (DTGS) detector and a sample shuttle accessory. Spectra were collected in the mid-IR spectral region (3,500-1,100 cm^{-1}) at sequential increments of temperature (5 to 90 $^{\circ}\text{C}$), allowing for equilibrium. Parameters for IR spectra data collection were the following 256 scans co-added apodized with a triangular function and Fourier transformed to provide a resolution of 4 cm^{-1} with data encoded every 2 cm^{-1} .

4.3.3 Data analysis

Peak maxima were determined for the amide I' and I*' regions for melittin, ^{13}C -*Cen* and ^{13}C -*Cen*/MLT complex (1:1, mol:mol). Spectral data analysis such as baseline correction and 2D-COS using a specialized computer program known as Kinetics for Matlab®, was generously provided by Dr. Erik Goormaghtigh from the Free University of Brussels, in Belgium.

4.4 Differential Scanning Calorimetry (DSC)

Calorimetric experiments were carried-out with a differential scanning micro-calorimeter model, VP-DSC (MicroCal, LLC, Northampton, MA) with a personal computer interface and the experimental parameters were defined using VP Viewer 2000-DSC-Origin 7 program. The up-scanning conditions were: scan rate 60 $^{\circ}\text{C}/\text{hr}$, 10 $^{\circ}\text{C}$ starting temperature;

127 °C final temperature; 16 sec. filtering period, and high feedback mode/gain were used for all samples.

The ^{13}C -*Cen*, melittin or ^{13}C -*Cen*/MLT complex were equilibrated using buffer containing 50 mM Hepes, 150 mM NaCl, 4 mM CaCl_2 and 4 mM MgCl_2 at pH 7.4. All samples and reference were degassed using Thermo Vac accessories and thermostated at 10 °C, before placing into the cells or injection syringe.

Approximately 1.201 mg/mL of melittin, 0.75 mg/mL of ^{13}C -*Cen*, or 1:1 molar ratio of ^{13}C -*Cen*/MLT mixture were injected in the sample cell. In the reference cell contained 0.5 ml of buffer solution (as described above).

The scanned plots were obtained using Micro Cal, LLC-DCS-Origin 7 program.

CHAPTER V

RESULTS AND DISCUSSIONS

5.1 Bacterial over-expression of ^{13}C -*Chlamydomonas* centrin

For the expression of full-length ^{13}C -*Chlamydomonas* centrin, *E. coli* BL21- λDE_3 cells were transformed with a pT7-5 plasmid. The newly transformed cells were grown using Bioflo 3000 fermentor in minimal media MARTEk 9 containing $> 98\%$ ^{13}C atom enrichment and 50 $\mu\text{g}/\text{mL}$ ampicillin. Bacterial growth was monitored by taking aliquots from the growth media every 30 minutes and measuring its optical density (O.D.) at 550nm. The bacterial cells were induced at mid-*log* phase (usually 2 hr from inoculation) with isopropyl- β -D-thiogalactopyranoside (IPTG) for the expression of ^{13}C -*Cen* (Fig. 5.1-1). Cells were harvested once they reached the stationary growth phase typically, 3.0 hrs from induction.

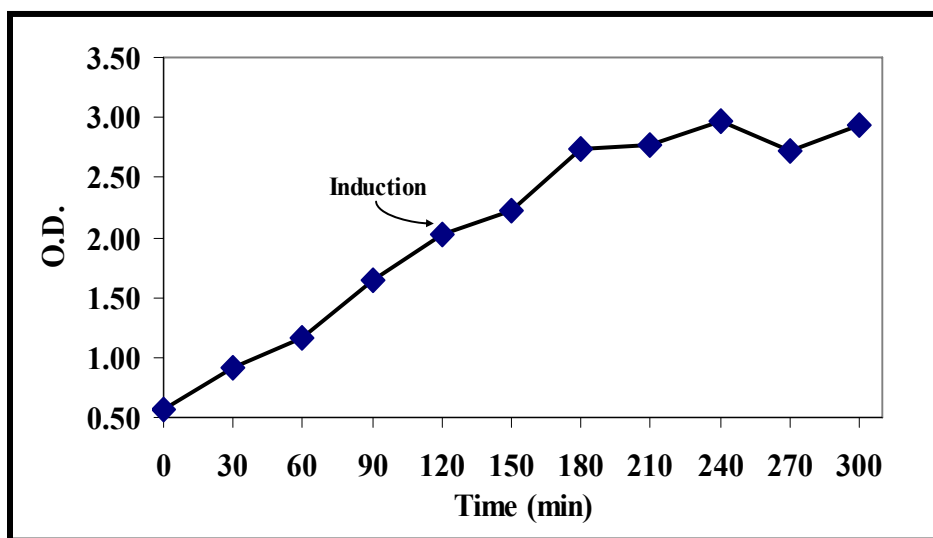


Figure 5.1-1 Growth curve of transformed *E. coli* BL21- λDE_3 over-expression of ^{13}C -*Chlamydomonas* centrin.

During the bacterial expression of ^{13}C -*Chlamydomonas* centrin, a high level of expression of centrin was observed by 5-15% SDS/PAGE. A time course of the expression of putative ^{13}C -*Cen* protein is shown in Figure 5.1-2. Following the addition of IPTG, aliquot samples were taken every 30 min. Over-expression of the 20 kDa ^{13}C -*Cen* was observed 30 min. after induction (t_3), and maximal expression was reached 3 hr. after induction (t_5).

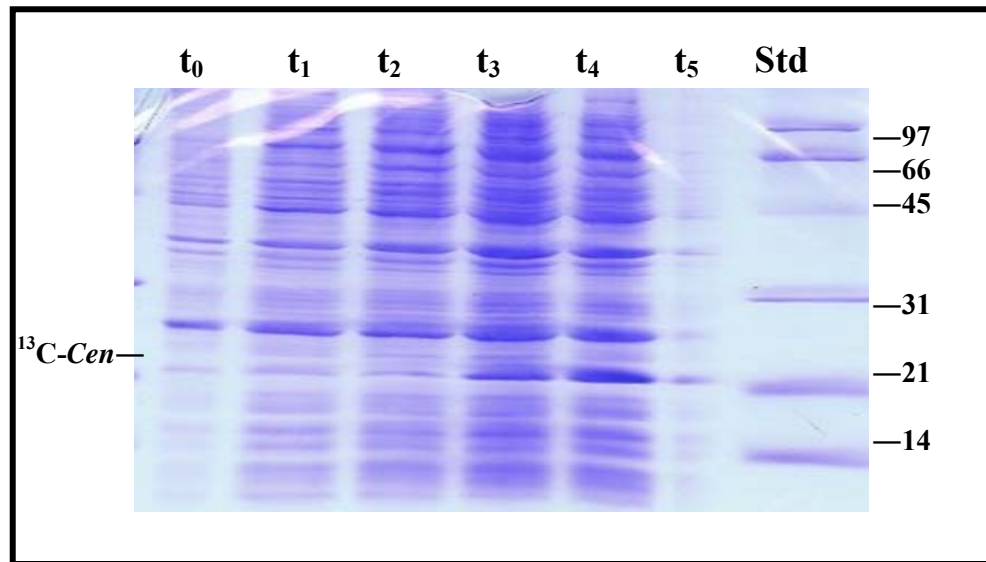


Figure 5.1-2 15% SDS-PAGE of ^{13}C -*Chlamydomonas* centrin expression. A coomassie blue-stained SDS-PAGE of the soluble proteins found in the bacterial cells lysates. At initial time (t_0), prior to inoculation (mid-*log* phase), (t_1 - t_2), prior to IPTG induction, (t_3 - t_5), after induction (stationary phase), and molecular weight standards (*Std*).

We obtained ~22.00 g of pellet that were harvested and frozen for the purification at a later time. Generally, the amount of pellet obtained in this type of expression is high when using enriched media (Pastrana-Ríos et al., 2001). In this isotope enriched minimal media, the bacterial growth is typically lower; and as a consequence the amount of pellet obtained was small.

5.2 Isolation and Purification of ^{13}C -*Chlamydomonas* centrin

5.2.1 Phenyl Sepharose CL4B Chromatography

Harvested *E. coli* BL21- λDE_3 cell pellets were lysed by brief sonication in lysis buffer at 4°C. After bacterial cell lysis and two centrifugation steps, the supernatant containing the soluble proteins and centrin were subjected to affinity chromatography. Figure 5.2-1 is a characteristic chromatogram where peak A indicates the void volume elution of low affinity (non-interacting) *E. coli* proteins. Elution with buffer containing EGTA and EDTA to chelate Ca^{+2} and Mg^{+2} , thus reducing the hydrophobic interactions with the column, and allowing for the elution of ^{13}C -*Cen* shown as peak B. Fractions collected within peak B curve were further analyzed by SDS-PAGE and U.V spectroscopy. Finally, peak C eluted other contaminants which had higher affinity for the column packing.

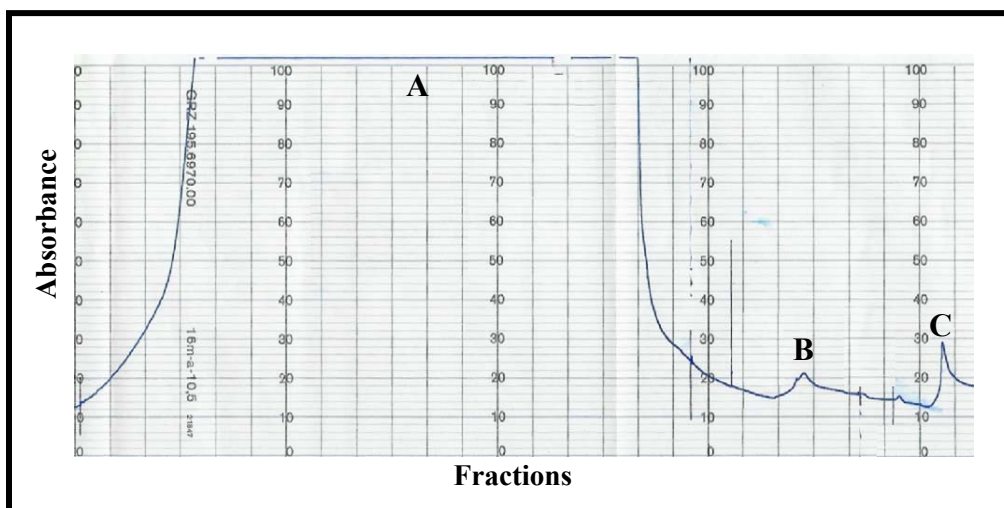


Figure 5.2-1 Phenyl sepharose chromatogram of purification of ^{13}C -*Chlamydomonas* centrin. Void volume (A), eluted fractions of ^{13}C -*Cen* and others protein that had similar interaction with the stationary phase (B) and other proteins contaminants with higher affinity for the stationary phase (C).

SDS-PAGE analysis of fractions collected during the phenyl sepharose chromatography containing different elution buffers were analyzed for protein content (Fig.5.2-2). The fractions eluted during peak A (lane A in Fig. 5.2-2) contain different constitutive bacterial proteins that do not have affinity for the stationary phase. Initial fractions collected in peaks B (lane B-B₁₂) were comprised of other bacterial proteins and fractions B₁₈-B₃₀ were positive for centrin. As a result, fractions containing centrin (B₁₅-B₆₀) were pooled, concentrated and buffer conditions exchanged to 40 mM Tris, 2 mM CaCl₂, 2 mM DTT and 0.08% NaN₃ and subjected to a second purification step: anion exchange chromatography.

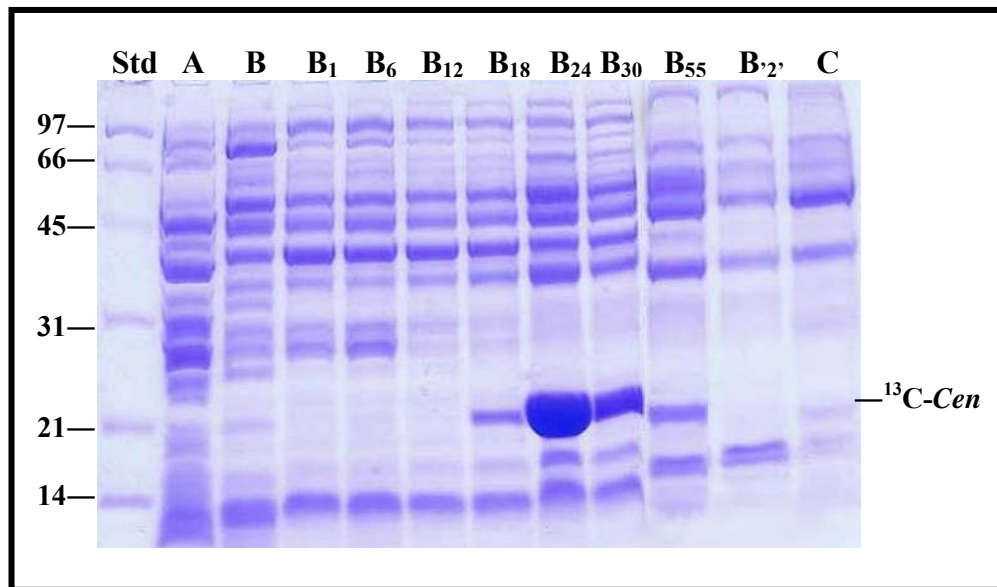


Figure 5.2-2 15% SDS-PAGE analysis of eluted fractions from phenyl sepharose column. SDS-PAGE of samples of different fraction collected during phenyl sepharose chromatography. Molecular wieght standards (Std), elution of bacterial cosntitutive proteins (A-B₁₂), elution of ¹³C-*Chlamydomonas* centrin is shown as an intense band at ~21 kDa and other proteins with similar affinity, (B₁₈-B₅₅), elution of other bacterial proteins (B₅₅-C).

5.2.2 Anion Exchange Chromatography

The positive fractions containing $^{13}\text{C-Cen}$ were concentrated, buffer exchanged and subjected to an anion exchange column chromatography. Elution of the desired protein was achieved using a NaCl gradient (0→0.75 M) and monitored at 280 nm (Fig.5.2-3). In peak A, eluted proteins do not interact (cationic proteins) with the column matrix, while anionic proteins such as $^{13}\text{C-Cen}$ bind to the cationic matrix. The elution of different anionic proteins occurs with increase salt concentration. Peaks B and C correspond to the elution of centrin according to gradient increase to 0 from 0.75 M of NaCl. Finally, peak D corresponds to other bacterial proteins.

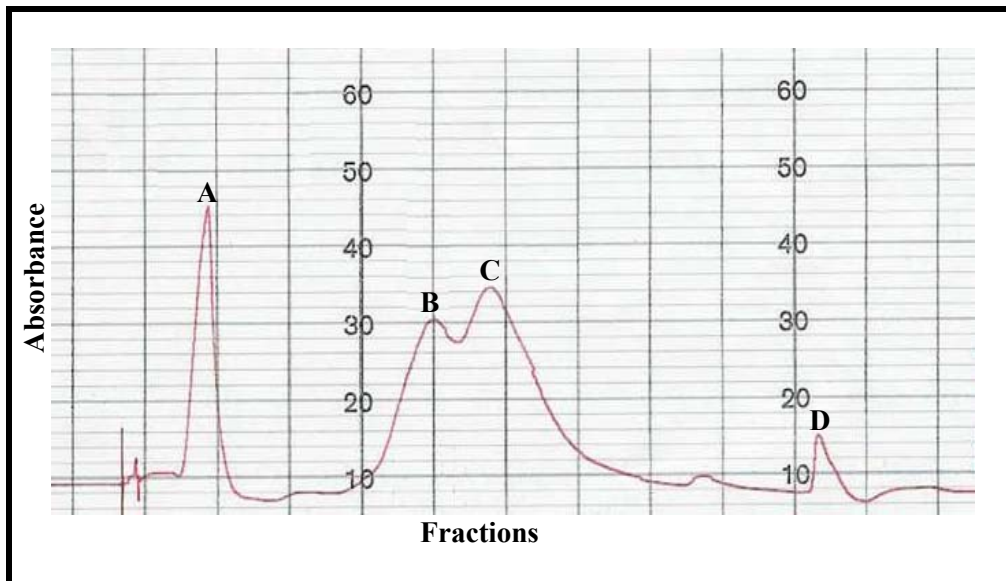


Figure 5.2-3 Anion exchange chromatogram (0-0.75 M NaCl) of the purification of $^{13}\text{C-Chlamydomonas centrin}$. Peak A, are cationic proteins elution, peaks B and C, elution comprised of different anionic proteins, $^{13}\text{C-Cen}$, and peak D remained bacterial proteins.

According to the elution pattern of peaks A, B, C and D fractions were pulled for SDS-PAGE analysis. Protein components for each set of fractions pooled are shown in Fig. 5.2-4; where initial fractions corresponding to bacterial cationic proteins (Lane 1-5, 6-10); while, anionic proteins such as ^{13}C -*Chlamydomonas* centrin (intense band \approx 20 kDa) eluted from fraction number 11 to the final fractions (Lane 11-16, 17-24).

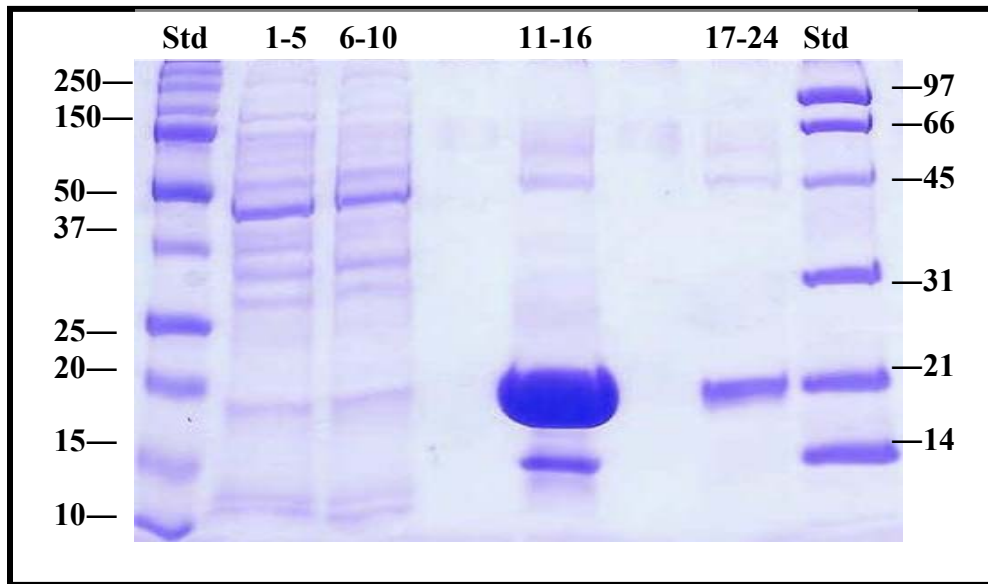


Figure 5.2-4 15% SDS-PAGE analysis after anionic chromatography for the purification of ^{13}C -*Chlamydomonas* centrin. Std, molecular weight standards, Lane 1-5 and 6-10, bacterial cationic proteins. An intense band corresponding to ^{13}C -*Chlamydomonas* centrin approximately 20 kDa are shown in lanes 11-16 and 17-24, together to anionic proteins.

Finally, small amounts of impurities were removed by dialysis (30 MW and 15 MW cut-off). SDS-PAGE analysis after dialysis was observed to contain a single band corresponding to ^{13}C -*Cen*, suggesting pure (>98%) protein was obtained (Fig. 5.2-5).

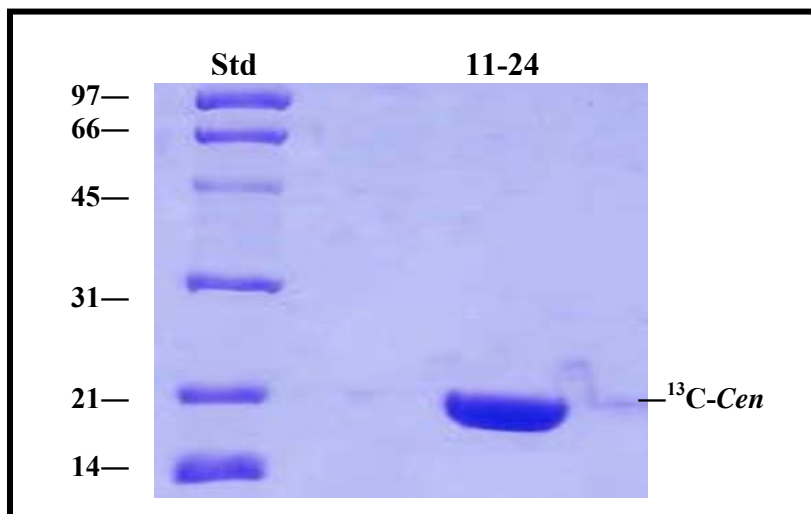


Figure 5.2-5 15% SDS-PAGE analysis of ¹³C-*Chlamydomonas* centrin > 98 % pure.

5.3 Ultra Violet Spectroscopic analysis

Fractions containing ¹³C-*Cen* were pooled and concentrated for UV spectral analysis. The spectrum acquired in the 241-300 nm spectral region shown in Figure 5.3-1, was comprised of three peak maxima at 252, 260 and 265 nm corresponding to phenylalanine, and a tyrosine peak at 274 nm. This is characteristic of ¹³C-*Chlamydomonas* centrin which is comprised of nine phenylalanine residues and one tyrosine in its sequence. The absence of tryptophan absorbance at 280 nm also indicated that the protein sample preparation did not contain other contaminating proteins.

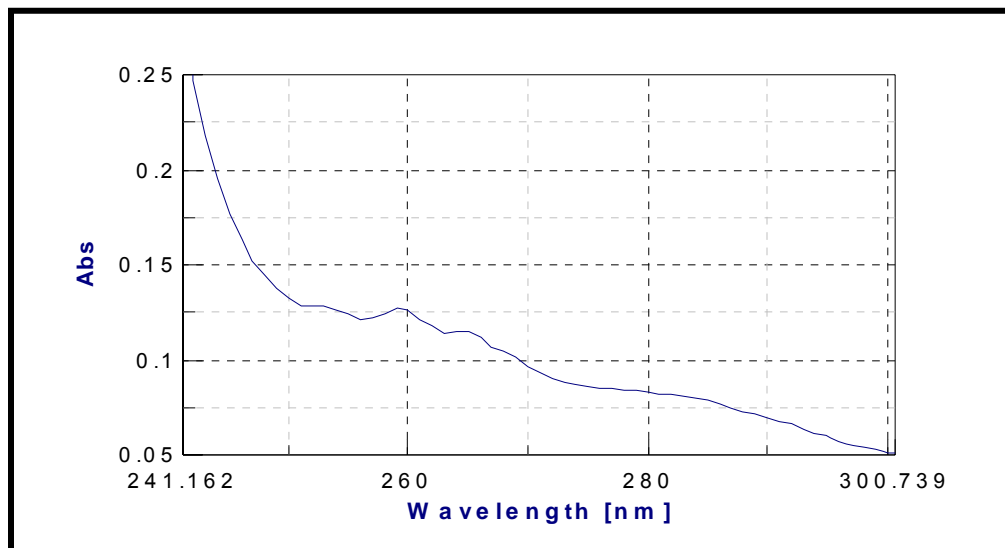


Figure 5.3-1 UV spectrum of ¹³C-*Chlamydomonas centrin*.

¹³C-*Cen* concentration was determined using direct UV absorbance at 274 nm after turbidity correction. The approximate amount of protein yield using the molar extinction coefficient of 1309.9 M⁻¹ cm⁻¹ was 4.17 mg. This yield was acceptable, since a minimal media was used for the expression of the desired recombinant protein. This protein was lyophilized and stored at -20 °C for its further use in biophysical studies.

5.4 Mass Spectrometry Analysis

To determine the purity, molecular weight, integrity and extent of isotopic incorporation a ¹³C-*Cen*, mass spectrometry analysis was carried-out. The protein sample was shipped to the protein Core Facility at Mayo Clinic and Foundation for ES-TOF-MS. Four peaks were observed (Fig. 5.4-1) with mass-to-charge ratio of 20130, 20145, 20185 and 20245. The differences of the mass-to-charge ratio can be due to grade of protonation of

protein, loss of one amino acid (average MW: 110 Da), or differences in calcium and magnesium state. The mass/charge difference of ^{13}C -Cen was approximately 839 Da when compared to the native protein (MW: 19,441 Da) due to the isotope content (^{13}C). More importantly, the absence of other peaks in the mass spectra confirmed its purity (> 98%), integrity, and homogeneous isotopic labeled state of ^{13}C -*Chlamydomonas* centrin.

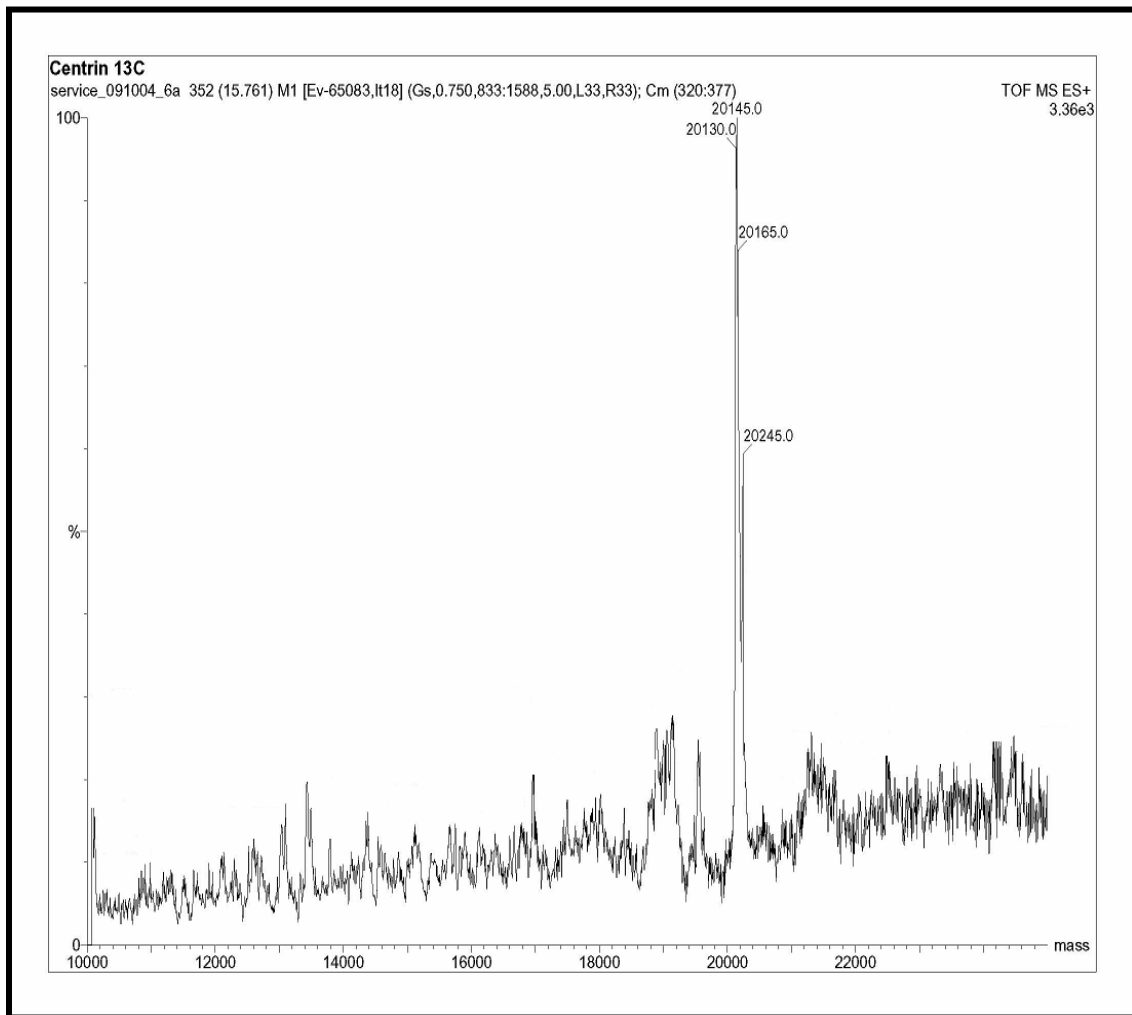


Figure 5.4-1 TOF-ES mass spectrometer of ^{13}C -*Chlamydomonas* centrin.

5.5 FT-IR Spectroscopy

5.5.1 H→D Exchange Analysis

The rate of H→D exchange is related to both the solvent accessibility of the N-H amide groups of the peptide bond, that are related to the secondary structure, and allowing for the determination of the proteins accessibility to its aqueous environment. For these H→D exchange studies in ^{13}C -Cen, melittin and ^{13}C -Cen/melittin complex, ATR-FT-IR spectra was acquired for a neat protein film in the spectral region of 1700-1400 cm^{-1} . This spectral region is comprised of the ^{13}C -Cen amide I* and I*' bands (1580-1670 cm^{-1}), MLT amide I and I' bands (1600-1700 cm^{-1}), and amide II and II' bands (1600-1400 cm^{-1}) observed for the complex, as shown in Figure 5.5-1. The typical spectral changes observed were due to the H/D exchange process. The amide I or I* band shifts to lower wavenumber from 1613 cm^{-1} to 1608 cm^{-1} for ^{13}C -Cen, from 1651 cm^{-1} to 1647 cm^{-1} for MLT, and from 1655 cm^{-1} to 1649 cm^{-1} for ^{13}C -Cen/MLT complex, accompanied by a decrease in intensity of the amide II band and simultaneous increase of the amide II' band is observed.

Difference spectra were generated by subtracting the first spectrum from all subsequent spectra to obtain the representative dynamic spectra or difference spectra (Fig. 5.5-1) which provided us with useful information: for ^{13}C -Cen shown in Fig. 5.5-1 A, we observed changes in intensity for the labeled random coil (r.c.) (1650 cm^{-1}), β -turns (1625 cm^{-1}), α -helix (1600 cm^{-1}), N-H deformation (1540 cm^{-1}), Tyr side chain (1515 cm^{-1}), and N-D deformation (1460 cm^{-1} , 1435 cm^{-1}). For melittin shown in Fig. 5.5-1 B, we observed changes in intensity of the α -helices (1655 cm^{-1} , 1640 cm^{-1}), N-H deformation (1545 cm^{-1}) and N-D deformation (1440 cm^{-1}). Finally, for ^{13}C -Cen/MLT complex shown in Fig. 5.5-1

C, we observed changes in intensity for melittin's overlapped α -helices (1650 cm^{-1} , 1640 cm^{-1}), $^{13}\text{C-Cen}$ overlapped unordered (1655 cm^{-1}), $^{13}\text{C-Cen}$ α -helix (1600 cm^{-1}), N-H deformation (1545 cm^{-1}) and N-D deformation (1430 cm^{-1}). The spectral feature changes observed the summaries above for the amide I band are typical for proteins hydrogen-deuterium exchange.

Moreover, by monitoring the amide II the intensity changes is possible to determine the kinetics of the exchange process.

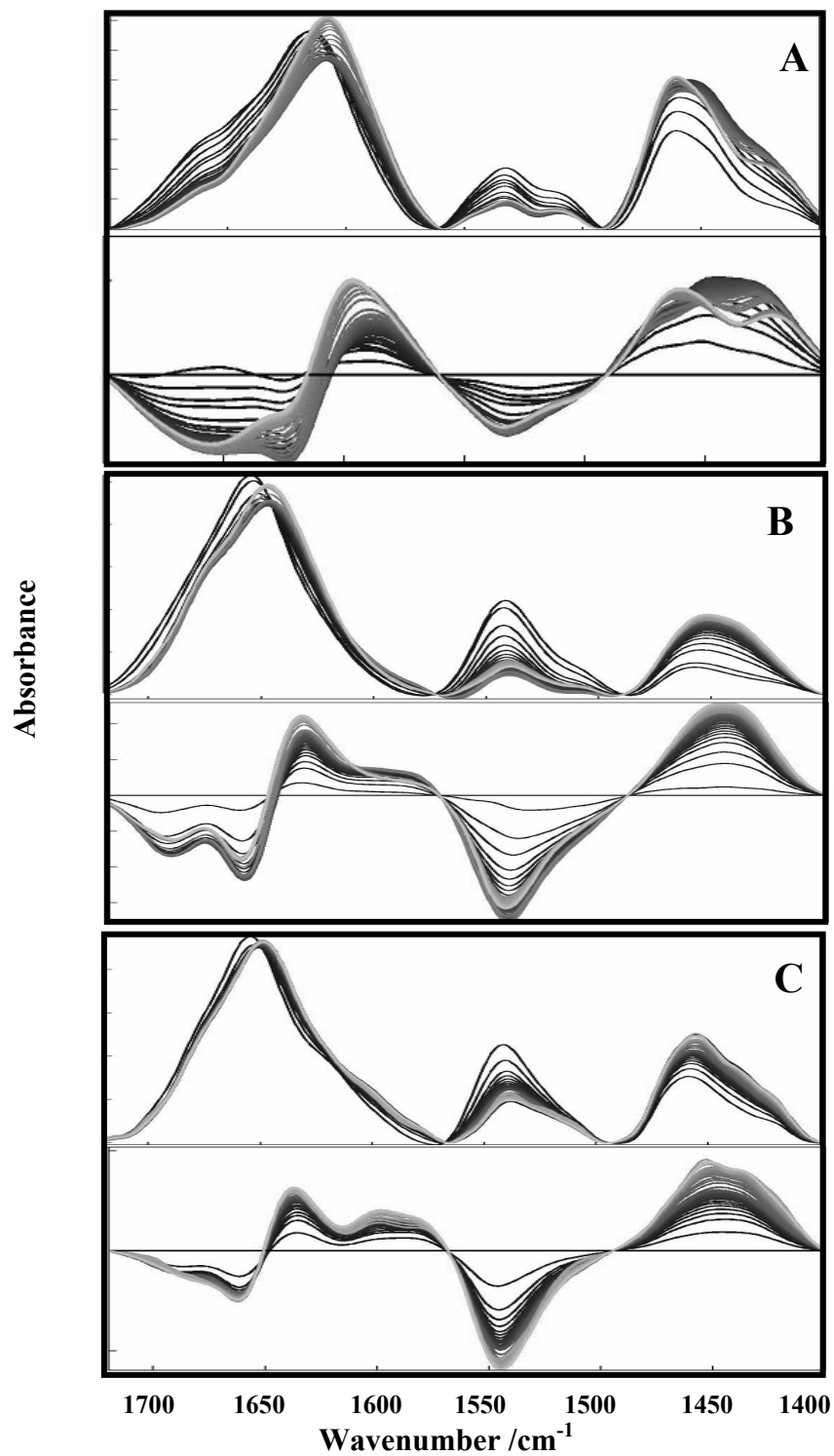


Figure 5.5-1 Overlaid and difference spectra in the region 1700-1400 cm^{-1} . (A) ^{13}C -Cen, (B) melittin, (C) ^{13}C -Cen/MLT complex. First spectrum (black line) and last spectrum (gray line).

5.5.2 Kinetics of exchange

H/D exchange of ^{13}C -*Cen*, MLT and ^{13}C -*Cen*/MLT complex were carried-out to determine the exchange rate constants for different secondary structural motifs, side chains and the overall extent of exchange. The single frequency kinetics for the determination of the number of variables and time constant needed to fit the evolution of the absorbance of the amide II/amide I' decay curve was plotted.

The analysis of the spectral data can be done per vibrational mode in a way that, the H/D exchange analysis will be specific for each structural motif and exchangeable side chains (Arg or Tyr). For the analysis, the isobestic points were determined for each spectral data set, to define the single frequency kinetics. The isobestic points were 1559 cm^{-1} (^{13}C -*Cen*), 1645 cm^{-1} (melittin), and 1651 cm^{-1} (^{13}C -*Cen*/MLT complex).

Kinetics of exchange were determined for each structural motif and compared with the complex to determine differences in solvent accessibility. We obtained the single frequency kinetics of the individual components and the complex, for which the evolution of the absorbance (amide II/amide I') was plotted (Fig. 5.5-2). This H/D exchange curve was fitted with a 3rd order exponential decay equation. In each case, the time constants and assignments were determined for ^{13}C -*Cen*: 0.40 min^{-1} for the fast component (random coil), 0.07 min^{-1} for the intermediated component (α -helix), and 0.003 min^{-1} for the slow component (Tyr and β -turns), while for melittin the time constants and assignments were: 0.50 min^{-1} for the fast component (turns), 0.01 min^{-1} for the intermediated component (α -helix), and 0.004 min^{-1} for the slow component (α -helix). Finally, for ^{13}C -*Cen*/MLT complex time constants and assignment were: 0.90 min^{-1} for the fast component (turns), 0.10 min^{-1} for

the intermediated component (α -helix (MLT)), and 0.002 for the slow component (α -helix ($^{13}\text{C-Cen}$)).

Figure 5.5-3 illustrates the extent of exchange for $^{13}\text{C-Cen}$, MLT and $^{13}\text{C-Cen/MLT}$ complex. For $^{13}\text{C-Cen}$ has 80% exchange within the first 15 min (Fig. 5.5-3 A) and did not vary until the end. Nevertheless, melittin and $^{13}\text{C-Cen/MLT}$ complex have 100% of deuteration within the first 20 min, showing a similar behavior (Fig. 5.5-3 B,C). This suggests that in presence of melittin, $^{13}\text{C-Cen}$ changes its conformation obtaining greater accessibility to solvent due to its interaction with the target peptide.

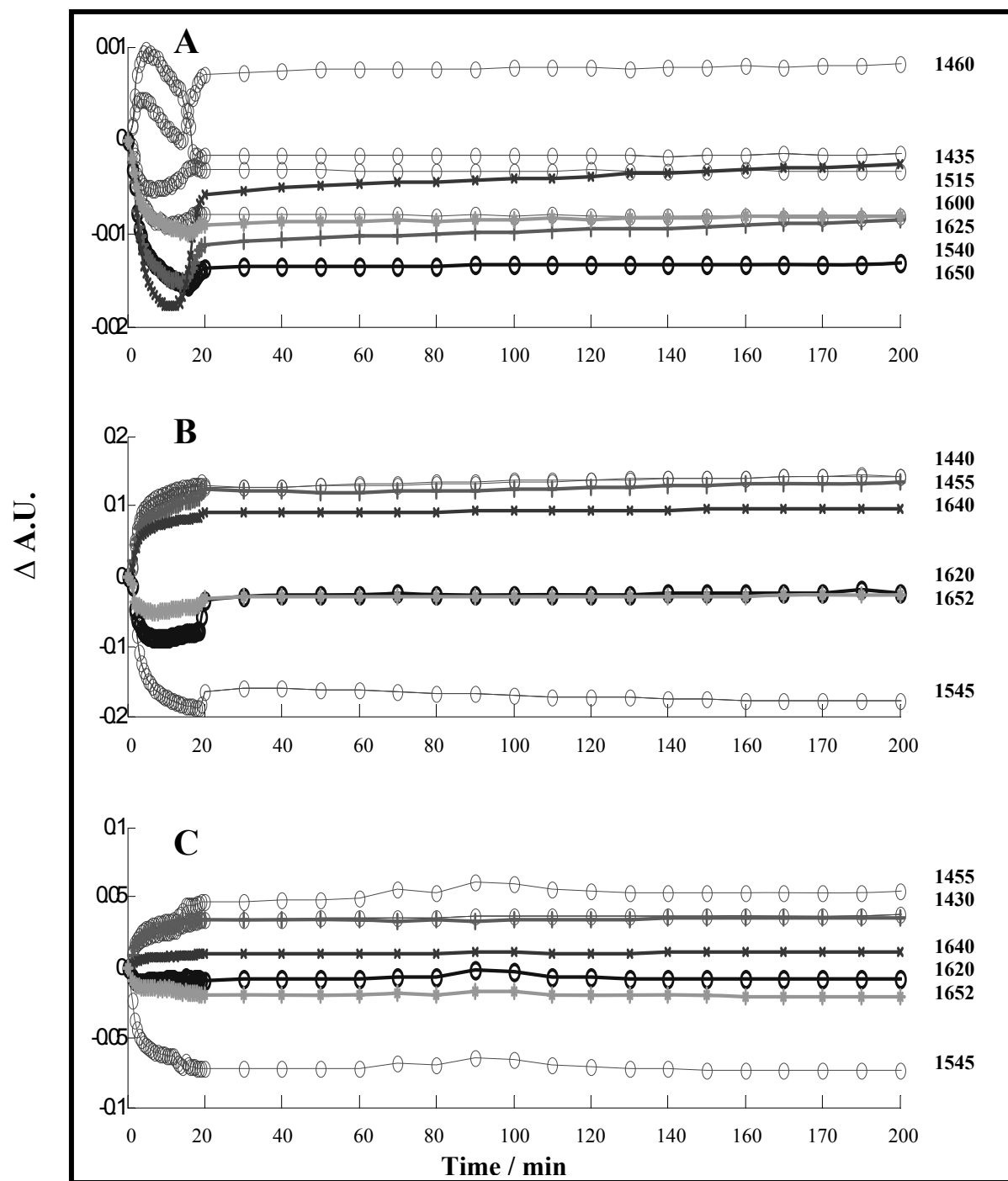


Figure 5.5-2 Single Frequency kinetics of individual components and the complex. Δ A.U. vs. times plots corresponding to: (A) ^{13}C -Cen, (B) melittin and (C) ^{13}C -Cen/MLT complex. The secondary structure: α -helix (-x-x-), random coil (+++), Tyr (1515 cm^{-1} , first plot), loops (‡‡‡), β -turns (†††) and NH/ND deformation (-o-o-).

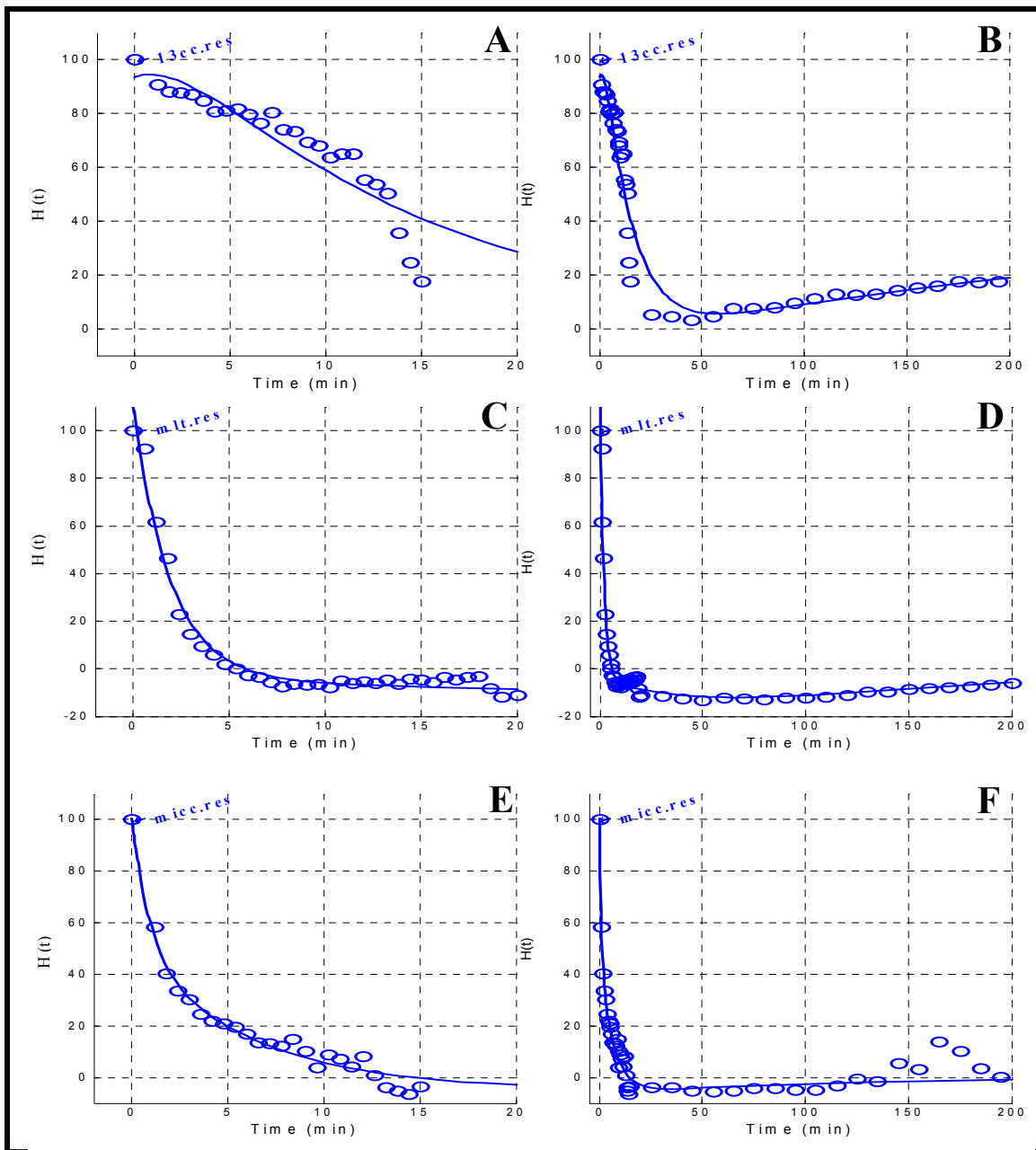


Figure 5.5-3 H→D exchange kinetics of $^{13}\text{C-Cen}$, melittin and $^{13}\text{C-Cen}$ complex. Extent of hydrogen exchange plots corresponding to: (A, B) $^{13}\text{C-Cen}$, (C, D) melittin and (E, F) $^{13}\text{C-Cen/MLT}$ complex. $^{13}\text{C-Cen}$ shows linear decay in the first 20 min with 80% of deuteration, while melittin and complex shows exponential decay and 100% of deuteration at 5 min and 15 min, respectively (A, C and E left plot respectively). In right plots shows final times of experiment with (A) 80% of deuteration in centrin and constant 100% of deuteration in (B) melittin and (C) complex, respectively.

5.5.3 Two Dimensional Correlation Analysis (2D-COS) during the H/D exchange process

To enhance the resolution of overlapping bands in the spectra and the characterization of the conformational changes in ^{13}C -*Cen*, melittin and the protein complex, a 2D-COS analysis was performed on each data set, within the spectral region of 1700-1400 cm^{-1} . The synchronous plots are shown in Figure 5.5-4 (A, B, C), and the asynchronous plots are shown in Figure 5.5-4 (D, E, F), for ^{13}C -*Cen*, melittin, and ^{13}C -*Cen*-MLT complex, respectively. The auto-peaks and cross peaks assignments are summarized in Table 5.5-1

Additionally in the analysis of synchronous plots in amide I' region for ^{13}C -*Cen*, three peaks were obtained: 1650 cm^{-1} , 1625 cm^{-1} , and 1600 cm^{-1} corresponding to unordered, β -turns, and α -helix secondary structure, respectively. For melittin two peaks were obtained: 1655 cm^{-1} and 1640 cm^{-1} corresponding to two types of α -helix structures. For ^{13}C -*Cen*/MLT complex two principal components were obtained: 1640 cm^{-1} and 1600 cm^{-1} , corresponding to α -helix of melittin contribution and α -helix of ^{13}C -*Cen* contribution, respectively.

On the other hand, the assignments and order of events of the exchange process were determined for each case (^{13}C -*Cen*, MLT, ^{13}C -*Cen*/MLT) by analyzing the asynchronous plots. These assignments are summarized in Table 5.5-2. In the analysis of the amide I band the order of events determined were the following: for ^{13}C -*Cen* α -helix, random coil (r.c.) and finally β -turns were exchanged; for melittin, α -helix at 1655 cm^{-1} prior to the helix at 1640 cm^{-1} , and for ^{13}C -*Cen*/MLT complex, concomitant exchange was observed for the MLT α -helix (1640 cm^{-1}) with ^{13}C -*Cen* α -helix (1600 cm^{-1}).

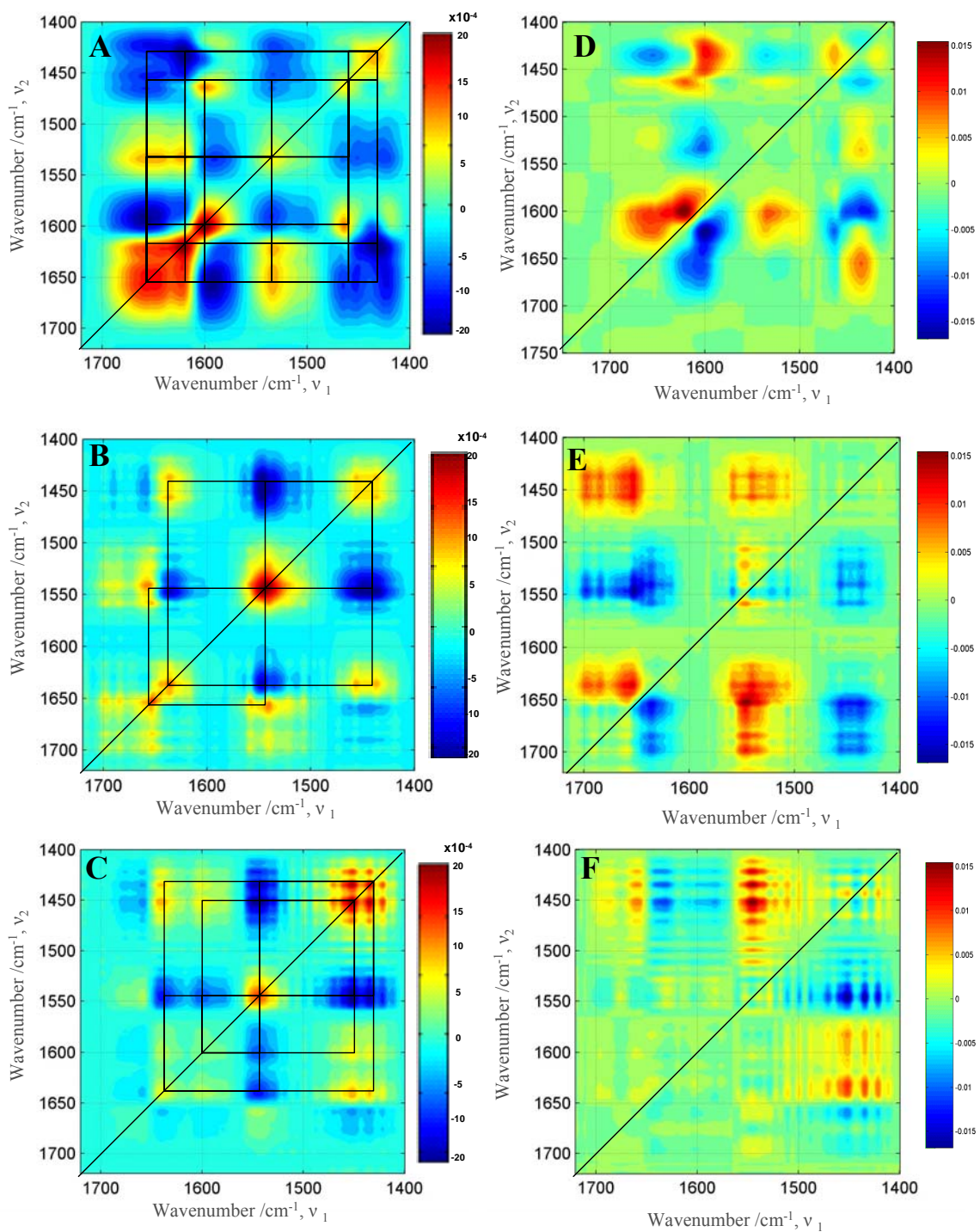


Figure 5.5-4 Synchronous and asynchronous contours plots corresponding to ^{13}C -*Chlamydomonas centrin* (A,D), melittin (B,E) and ^{13}C -Cen/MLT complex (C, F).

Table 5.5-1 2D-COS assignments of the synchronous and asynchronous plots for ^{13}C -*Chlamydomonas* centrin, melittin and ^{13}C -Cen/MLT complex.

Assignment	^{13}C - <i>Chlamydomonas</i> centrin		Melittin		^{13}C -Cen/MLT complex	
	Synchronous auto-peaks /cm ⁻¹	Asynchronous cross-peaks /cm ⁻¹	Synchronous auto-peaks / cm ⁻¹	Asynchronous cross-peaks /cm ⁻¹	Synchronous auto-peaks /cm ⁻¹	Asynchronous cross-peaks /cm ⁻¹
Random coil (r.c)	1650	1655	--- ^(a)	--- ^(a)	--- ^(a)	--- ^(a)
β -turns	1625	1625	--- ^(a)	--- ^(a)	--- ^(a)	--- ^(a)
α -helix (^{13}C)	1600	1598	--- ^(a)	--- ^(a)	1600	1600
α -helix (MLT)	--- ^(a)	--- ^(a)	1655-1640	1650-1640	1640	1640
Tyr side chain	1515	1510	--- ^(a)	--- ^(a)	--- ^(a)	--- ^(a)
N-H deformation	1540	1540	1545	1550	1545	1550
N-D deformation	1460	1450	1455	1450	1455	1450

^(a) N/A

Table 5.5-2 Summary of phase analysis used to determine H→D exchange dynamics in ¹³C-*Chlamydomonas* centrin, melittin and ¹³C-Cen/MLT complex.

Asynchronous plots analysis	
Events	
¹³C-<i>Chlamydomonas</i> centrin	
1	r.c. (1650 cm ⁻¹) occurs before N-D (1460 cm ⁻¹)
2	r.c. (1650 cm ⁻¹) occurs before N-H (1540 cm ⁻¹)
3	α-helix (1600 cm ⁻¹) occurs before r.c. (1650cm ⁻¹)
4	turns-β (1625 cm ⁻¹) occurs after N-D (1460 cm ⁻¹)
5	α-helix (1600 cm ⁻¹) occurs before turns-β (1625 cm ⁻¹)
6	α-helix (1600 cm ⁻¹) occurs after N-H (1540 cm ⁻¹)
Melittin	
1	α-helix (1655 cm ⁻¹) occurs after N-D (1440 cm ⁻¹)
2	α-helix (1655 cm ⁻¹) occurs after N-D (1455 cm ⁻¹)
3	α-helix (1655 cm ⁻¹) occurs before α-helix (1640 cm ⁻¹)
¹³C-Cen/MLT complex	
1	α-helix (MLT) (1640 cm ⁻¹) occurs after N-D (1455 cm ⁻¹)
2	α-helix (C) (1600 cm ⁻¹) occurs after N-D (1455 cm ⁻¹)
3	N-D (1455 cm ⁻¹) occurs before N-H (1545 cm ⁻¹)

5.6 Thermal Dependence Studies

FT-IR transmission spectroscopy was used to study the molecular changes that occur in ^{13}C -*Cen*, melittin and ^{13}C -*Cen*/MLT complex during a thermal perturbation. The infrared amide I' (MLT) and amide I*' (^{13}C -*Cen*) bands located between 1700-1550 cm^{-1} in D_2O are due to C=O stretching vibration of the peptide bond. This vibrational mode is sensitive to conformational changes and can be used to monitor any changes in the secondary structure composition of the complex and its components.

The spectra obtained for ^{13}C -*Chlamydomonas* centrin, melittin and ^{13}C -*Cen*/MLT complex as a function of temperature (20-95 $^{\circ}\text{C}$) in the presence of calcium are shown in Figure 5.6-1. For ^{13}C -*Cen* we can observe the shift and intensity decrease of the α -helical band ($\sim 1590\text{ cm}^{-1}$) and the intensity increase of the β -turns (1620 cm^{-1}) and random coil (r.c.) band ($\sim 1635\text{ cm}^{-1}$) for the amide I*' band (Fig. 5.6-1A). While, for melittin the changes observed are: intensity decrease of the α -helical band (1640 cm^{-1}) and intensity increase for the random coil (1690 cm^{-1}) and loop (1670 cm^{-1}) bands shown in Fig. 5.6-1B. For ^{13}C -*Cen*/MLT complex the changes observed are: intensity decrease of the α -helical band corresponding to ^{13}C -*Cen* (1590 cm^{-1}); the center band is a combination of the following contributions of α -helices of melittin (1630 cm^{-1}) and ^{13}C -*Cen* random coil (1630 cm^{-1}). In addition, intensity increases were observed for β -turns (1620 cm^{-1}) and random coil (1695 cm^{-1}) bands corresponding to ^{13}C -*Cen* in amide I*' and melittin in amide I' bands, respectively (Fig. 5.6-1C).

Furthermore, we compared the change of the spectral features during the thermal dependence study at low and high calcium concentrations (0.2 mM and 4 mM), in ^{13}C -*Cen*

and ^{13}C -*Cen*/MLT complex (Fig. 5.6-2). There are defined changes in the spectrum due to the presence of cations at 25°C. The amide I* band is shifted by 10 cm^{-1} , from 1590 cm^{-1} to 1600 cm^{-1} and the random coil (1630 cm^{-1}) and loop (1620 cm^{-1}) band intensity decreased with increased calcium concentrations (Fig. 5.6-2A). For ^{13}C -*Cen* a similar behavior was observed for ^{13}C -*Cen*/MLT complex (Fig. 5.6-2C). More importantly, at 80 °C we observed greater stability of ^{13}C -*Cen* in the presence of melittin.

These results suggest that high Ca^{+2} concentrations stabilized the protein (^{13}C -*Cen*) during the thermal perturbation in agreement with Pastrana et al., 2002 for the comparative study of apo and holo-centrin thermal dependence study. Also, our results with ^{13}C -*Cen*/MLT complex are in agreement with Hu et al., 2004 for the ^{15}N -centrin carboxy terminal domain/Kar1p complex, suggesting that centrin is stabilized in presence of a target peptide.

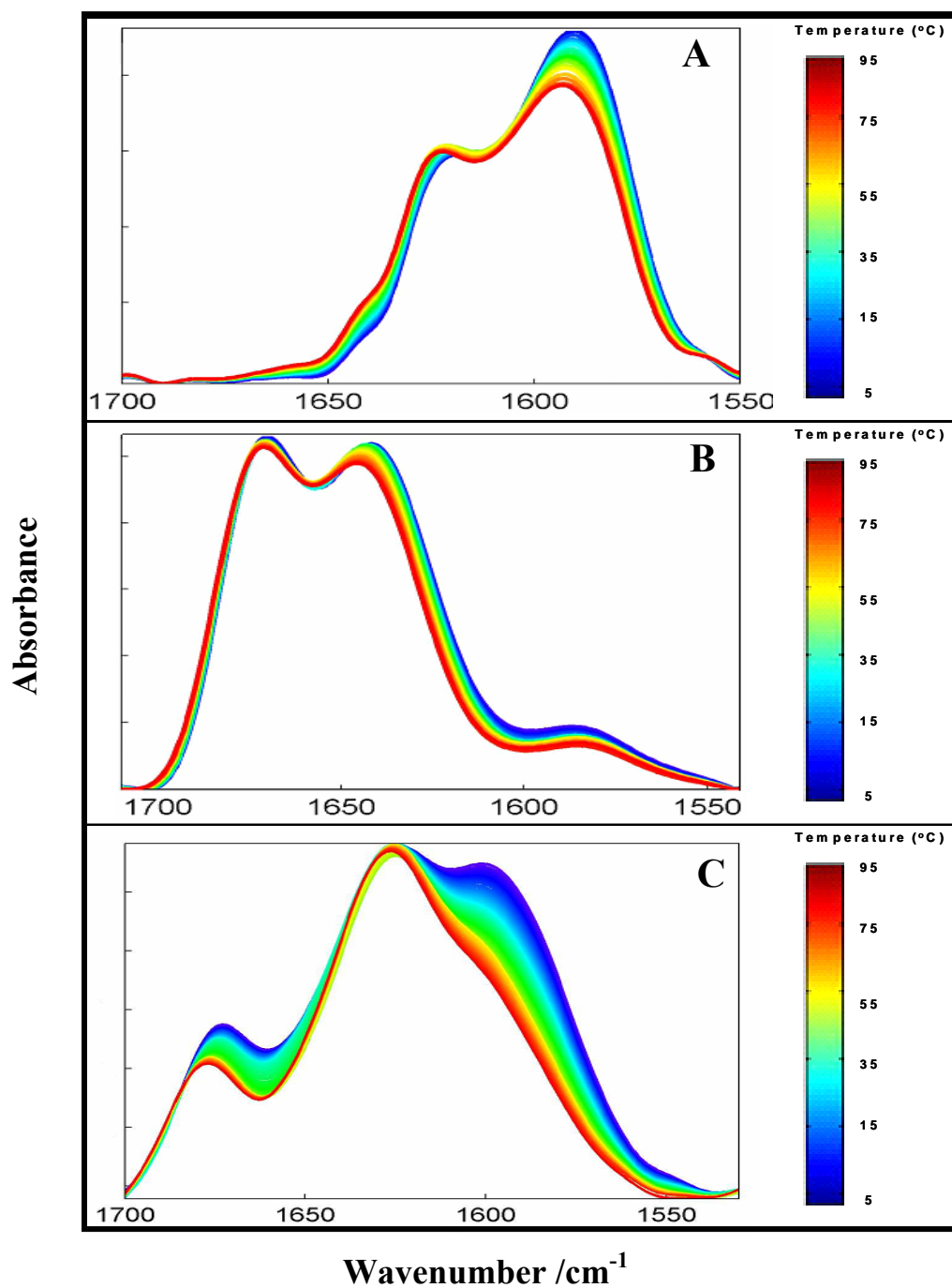


Figure 5.6-1 Overlaid FT-IR spectra of (A) ^{13}C -Cen, (B) melittin and (C) ^{13}C -Cen/MLT complex. Spectral features changes of the amide I' and I*' due to increased temperature (20 °C - 90 °C) in the spectral region 1700-1550 cm^{-1} . The side bar indicates the color correspondence with temperature.

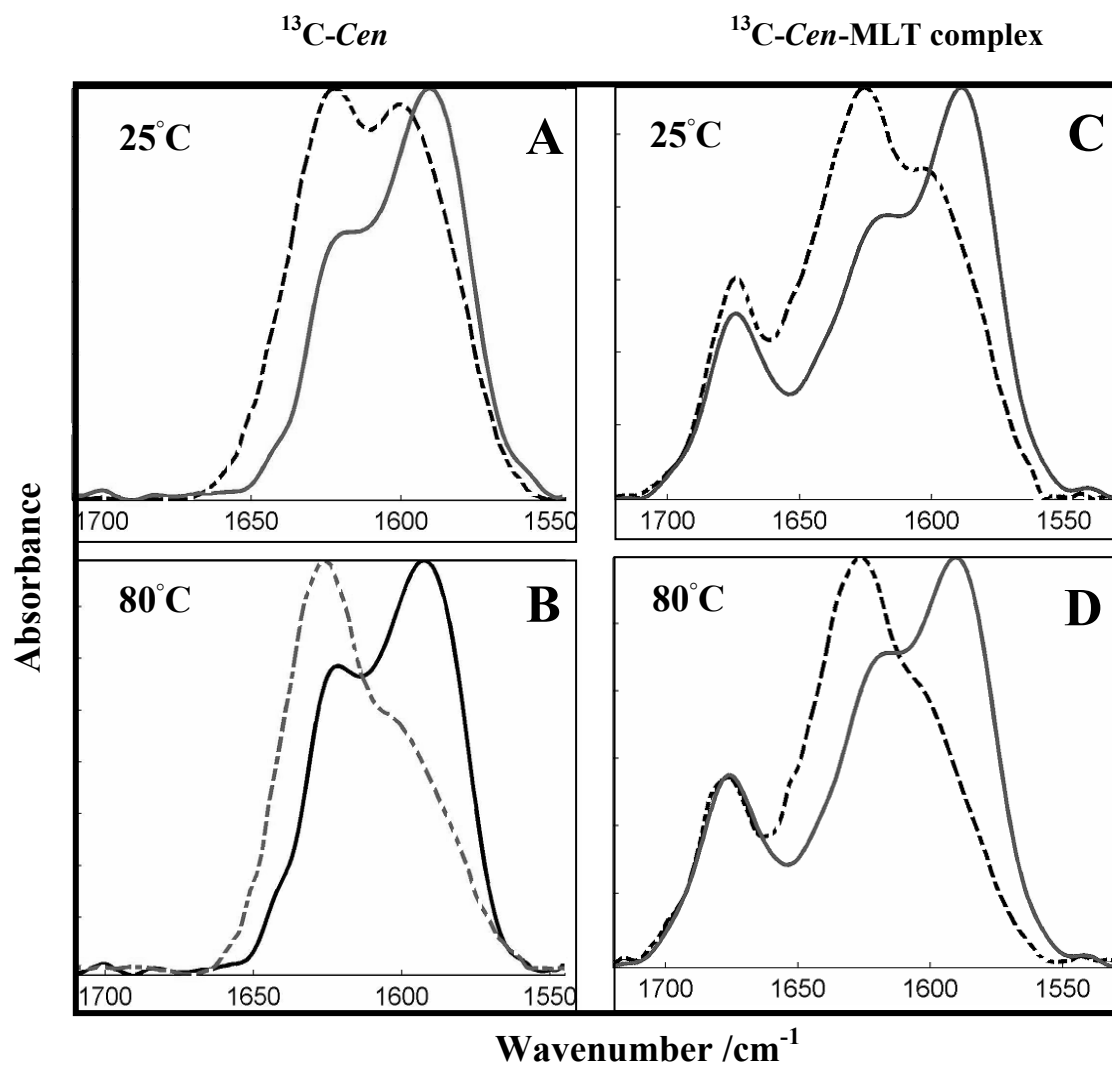


Figure 5.6-2 Overlaid FT-IR spectra of ^{13}C -*Chlamydomonas* centrin and ^{13}C -Cen/MLT complex at two calcium concentration. 4 mM CaCl_2 (—) and 0.2 mM CaCl_2 (---): (A,B) ^{13}C -Cen at 25 °C and 80 °C, respectively, (C,D) ^{13}C -Cen/MLT complex at 25 °C and 80 °C, respectively.

5.6.1 Two dimensional correlation analysis

Two dimensional correlation analysis was performed to enhance the resolution of the ^{13}C -*Cen*, MLT and complex amide I bands observed in the one-dimensional spectrum. Also, establish if coupling of the vibrational modes are due to ^{13}C -*Cen*/MLT interaction. Furthermore, with this analysis we can establish the order of events during the thermal dependence study and establish relative stability in the single component and in the complex. In general, a position specific thermal unfolding study was carried-out by monitoring the auto-peaks and cross-peaks associated with the amide I' and I'* bands, that include vibrational modes sensitive to secondary structure changes. Results obtained in the synchronous and asynchronous maps for ^{13}C -*Cen*, melittin and ^{13}C -*Cen*/MLT complex are shown in Figure 5.6-3.

Analysis of synchronous plots, contain positive auto peaks on the diagonal; these peaks are the vibrational modes that are being perturbed. Off diagonal positive peaks, known as cross-peaks indicate that the reorientation is in phase while, the negative cross-peaks represent decrease intensity. In figure 5.6-3 A for ^{13}C -*Cen* three auto peaks were observed at 1580 cm^{-1} (α -helix*), 1630 cm^{-1} (β -sheet*) and 1640 cm^{-1} (r.c.*). In addition, a negative cross peak correlating the 1640 cm^{-1} (r.c.*) with 1580 cm^{-1} (α -helix*) was observed. This indicates that changes in intensity are occurring out of phase i.e. α -helix intensity decreases while, random coil intensity increases. In Figure 5.6-3 B, three auto peaks are observed 1635 cm^{-1} (α -helix), 1670 cm^{-1} (β -turn) and 1690 cm^{-1} (r.c.). Furthermore, three cross peaks are observed at 1670 cm^{-1} (β -turn) correlating with 1690 cm^{-1} (r.c.), 1635 cm^{-1} (α -helix) correlating with 1690 cm^{-1} (r.c.), and the third cross peak is also at 1635 cm^{-1} (α -helix)

correlating with 1670 cm^{-1} (β -turn). For the complex we observed that MLT is indeed interacting with centrin (Fig. 5.6-3 C). The auto peaks observed are 1590 cm^{-1} (^{13}C -Cen α -helix), 1630 cm^{-1} (overlapped ^{13}C -Cen β -sheet and MLT α -helix) 1670 cm^{-1} (MLT β -turn) 1690 cm^{-1} (MLT r.c.). There are two additional cross peaks when compared to ^{13}C -Cen and MLT single components suggesting interaction between centrin and melittin. These cross peaks are positive phase 1590 cm^{-1} (^{13}C -Cen α -helix) correlating with 1660 cm^{-1} (MLT β -turn) and a negative phase cross peak at 1590 cm^{-1} (^{13}C -Cen α -helix) correlating with the 1690 cm^{-1} (MLT r.c.).

Asynchronous plots were used to determine chronological order of the events that occurred during the thermal perturbation. The peak assignments for each sample preparation are summarized in Table 5.6-1 and the sequence of the thermal perturbation events in each case are summarized in Table 5.6-2. For ^{13}C -Cen (Fig. 5.6-3 D), all of the cross peaks were positive except for 1585 cm^{-1} (Arg) which correlated with 1578 cm^{-1} (Asp $^-$). The positive cross peaks are 1630 cm^{-1} (β -sheet) correlated with three peaks 1611 cm^{-1} (Arg), 1590 cm^{-1} (α -helix) and 1580 cm^{-1} (Asp $^-$); 1618 cm^{-1} (α -helix) correlated with 1590 cm^{-1} (α -helix); 1600 cm^{-1} correlated with two peaks 1590 cm^{-1} (α -helix) and 1578 cm^{-1} (Asp $^-$); and 1578 cm^{-1} (Asp $^-$) correlated with 1565 cm^{-1} (Glu $^-$). For MLT shown in Figure 5.6-3 E, three cross peaks were observed 1690 cm^{-1} (MLT r.c.) correlated with 1630 cm^{-1} (α -helix); 1640 cm^{-1} (α -helix) is correlated with three peaks 1630 cm^{-1} (α -helix), 1600 cm^{-1} and 1590 cm^{-1} (Arg modes).

For the complex seven cross peaks are observed in Figure 5.6-3 F: 1690 cm^{-1} (MLT r.c.) correlated with two peaks 1630 cm^{-1} (MLT α -helix) and 1590 cm^{-1} (^{13}C -Cen α -helix);

1670 cm^{-1} (MLT β -turn) correlated with three peaks 1630 cm^{-1} (MLT α -helix), 1590 cm^{-1} ($^{13}\text{C-Cen}$ α -helix) and 1565 cm^{-1} ($^{13}\text{C-Cen}$ Glu $^-$); 1630 cm^{-1} (MLT α -helix) is correlated with three peaks 1590 cm^{-1} ($^{13}\text{C-Cen}$ α -helix) 1610 cm^{-1} (MLT and $^{13}\text{C-Cen}$ Arg) and 1565 cm^{-1} ($^{13}\text{C-Cen}$ Glu $^-$); 1590 cm^{-1} ($^{13}\text{C-Cen}$ α -helix) with 1565 cm^{-1} ($^{13}\text{C-Cen}$ Glu $^-$).

The phase analysis rendered the following order of events: for $^{13}\text{C-Cen}$ was random coil (1635 cm^{-1}), loops (1583 cm^{-1}), followed to Asp $^-$ (1578 cm^{-1}), β -turns (1620 cm^{-1}), and finally α -helix (1595 cm^{-1}). For melittin the following order of events: Arg (1586 cm^{-1}), loops (1670 cm^{-1}), random coil (1690 cm^{-1}) and finally α -helix (1640 cm^{-1}) were observed. While for $^{13}\text{C-Cen/MLT}$ complex was: random coil of melittin (1695 cm^{-1}) and $^{13}\text{C-Cen}$ (1665 cm^{-1}), Arg (1580 cm^{-1}) and finally α -helices corresponding to $^{13}\text{C-Cen}$ (1590 cm^{-1}) and melittin (1630 cm^{-1}) in the complex.

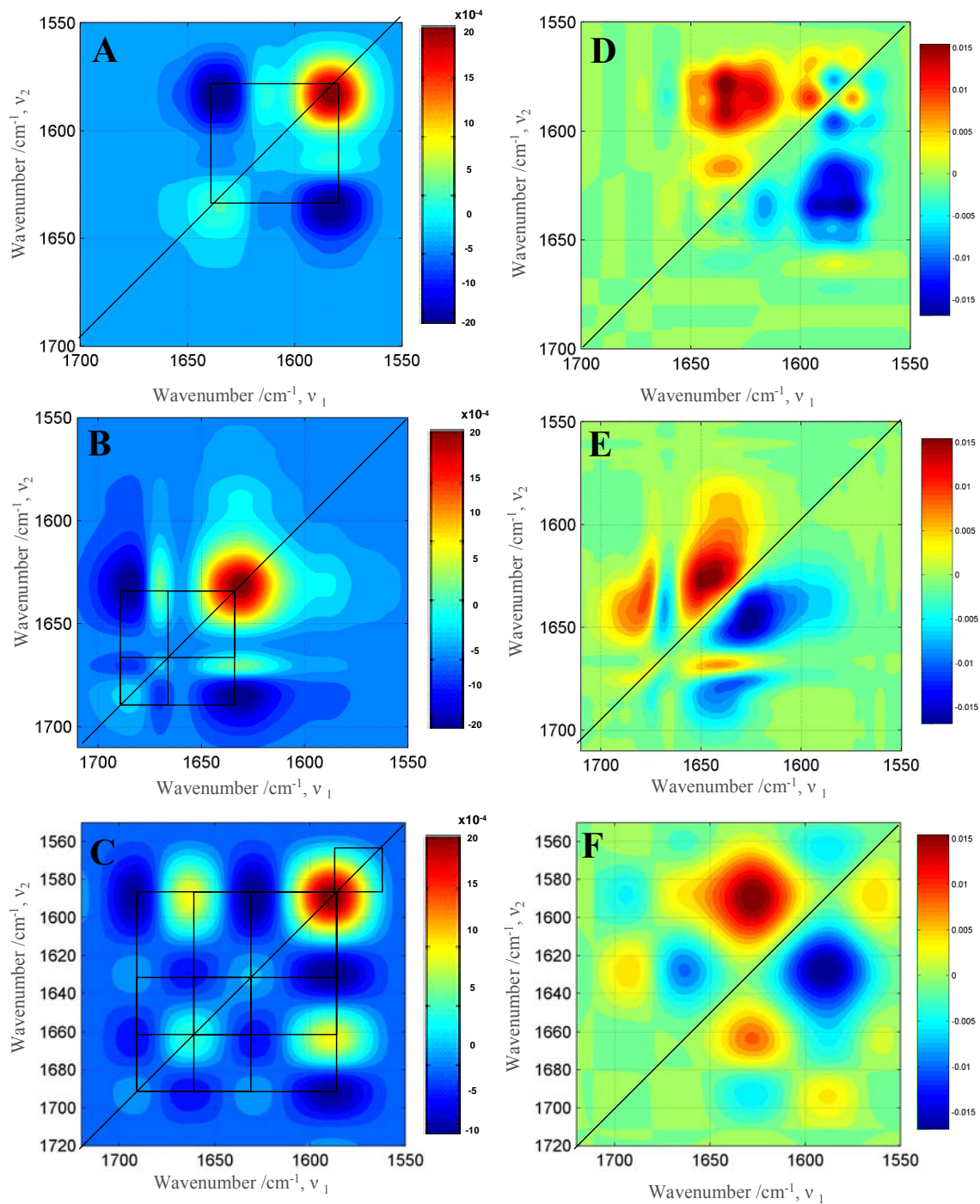


Figure 5.6-3 Synchronous and asynchronous contours plots corresponding to (A, D) ^{13}C -*Chlamydomonas* centrin, (B, E) melittin and (C,F) ^{13}C -Cen/MLT complex.

Table 5.6-1 Summary of phase analysis used for thermal characterization in ^{13}C -*Chlamydomonas centrin*, melittin and ^{13}C -*Cen*/MLT complex.

Events	Asynchronous plots analysis
^{13}C-<i>Chlamydomonas centrin</i>	
1	Asp (1578 cm^{-1}) occurs after random coil (1635 cm^{-1})
2	Asp (1578 cm^{-1}) occurs after loops (1583 cm^{-1})
3	loops (1583 cm^{-1}) occurs before α -helix (1595 cm^{-1})
4	α -helix (1595 cm^{-1}) occurs after β -turns (1620 cm^{-1})
5	loops (1583 cm^{-1}) occurs before α -helix (1595 cm^{-1})
6	α -helix (1595 cm^{-1}) occurs after random coil (1635 cm^{-1})
7	β -turns (1620 cm^{-1}) occurs after random coil (1635 cm^{-1})
Melittin	
1	Arg (1586 cm^{-1}) occurs after α -helix (1640 cm^{-1})
2	α -helix (1640 cm^{-1}) occurs after random coil (1690 cm^{-1})
3	Arg (1586 cm^{-1}) occurs before random coil (1690 cm^{-1})
^{13}C-<i>Cen</i>/MLT complex	
1	r.c. (MLT) (1695 cm^{-1}) occurs before α -helix (^{13}C - <i>Cen</i>) (1590 cm^{-1})
2	α -helix (MLT) (1630 cm^{-1}) occurs before r.c. (MLT) (1695 cm^{-1})
3	r.c. (^{13}C - <i>Cen</i>) (1665 cm^{-1}) occurs before α -helix (^{13}C - <i>Cen</i>) (1590 cm^{-1})
4	r.c. (^{13}C - <i>Cen</i>) (1665 cm^{-1}) occurs before α -helix (MLT) (1630 cm^{-1})
5	α -helix (^{13}C - <i>Cen</i>) (1590 cm^{-1}) occurs before r.c. (^{13}C - <i>Cen</i>) (1630 cm^{-1})
6	α -helix (^{13}C - <i>Cen</i>) (1590 cm^{-1}) occurs before r.c. (MLT) (1665 cm^{-1})
7	r.c. (^{13}C - <i>Cen</i>) (1665 cm^{-1}) occurs before α -helix (^{13}C - <i>Cen</i>) (1590 cm^{-1})
8	Arg (1580 cm^{-1}) occurs before α -helix (^{13}C - <i>Cen</i>) (1590 cm^{-1})

Table 5.6-2 Summary of secondary structure assignment obtained from the synchronous and asynchronous plots for ^{13}C -*Chlamydomonas* centrin, melittin and ^{13}C -Cen/MLT complex.

Assignment	^{13}C - <i>Chlamydomonas</i> centrin		Melittin		^{13}C -Cen/MLT complex	
	Synchronous auto-peaks /cm ⁻¹	Asynchronous cross-peaks /cm ⁻¹	Synchronous auto-peaks / cm ⁻¹	Asynchronous cross-peaks /cm ⁻¹	Synchronous auto-peaks /cm ⁻¹	Asynchronous cross-peaks /cm ⁻¹
*Random coil (<i>rc</i>) (^{13}C -Cen)	1640	1635	---(a)	---(a)	1660	1665
Random coil (MLT)	---(a)	---(a)	1690	1690	1693	1695
β-turns	---(a)	1620	---(a)	---(a)	---(a)	---(a)
loops	---(a)	1583	1670	1670	---(a)	---(a)
*α-helix (^{13}C -Cen)	1583	1595	---(a)	---(a)	1590	1590
α-helix (MLT)	---(a)	---(a)	1630	1640	1629	1630
Arg side chain	---(a)	---(a)	1590	1586	1585	1580
Asp side chain	---(a)	1578	---(a)	---(a)	---(a)	---(a)

(a) N/A

*Shifts due to isotope labeling.

5.6.2 Thermal Dependence Studies

The maximum peak (Fig. 5.6-1) for the amide I' and I'* bands of the FT-IR spectra for $^{13}\text{C-Cen}$, MLT and the complex for 0.2 mM and 4 mM of calcium were plotted as a function of the temperature (20 - 90 °C). The maximum peaks corresponds to α -helix* ($^{13}\text{C-Cen}$, ~1590 or 1602 cm^{-1}), β -sheet ($^{13}\text{C-Cen}$, ~1616 or 1624 cm^{-1}), α -helix (MLT ~1627 cm^{-1}), and a combination of the above peaks within the complex, in panels A, B, C and D (Fig. 5.6-4).

For $^{13}\text{C-Cen}$ two pre-transitions at 30 °C and 60 °C at 0.2 mM Ca^{+2} were observed while, only a linear transition at 4 mM Ca^{+2} was observed for the α -helix*(middle open and closed circle at 0.2mM Ca^{+2} and 4mM Ca^{+2} , respectively Fig. 5.6-4 A,B). On the other hand, the β -sheet*, one pre-transition at 80 °C and 30 °C at 0.2 mM Ca^{+2} and 4 mM Ca^{+2} , respectively were observed. Again, these results indicated that $^{13}\text{C-Cen}$ in the presence of high calcium concentration (holo- form) was more stable.

However, in the analysis of peak maximum within the complex (closed and middle open circle at 0.2mM Ca^{+2} and 4mM Ca^{+2} , respectively) one pre-transition at 55°C and 65°C for α -helix* regions at 0.2 mM Ca^{+2} and 4mM Ca^{+2} , respectively was observed (Fig. 5.6-4 A, B). While, two pre-transitions 30 °C, 70 °C at 0.2 mM Ca^{+2} and two pre-transitions 35 °C, 70 °C at 4 mM Ca^{+2} were observed for the α -helix of melittin and β -sheet* of $^{13}\text{C-Cen}$ during the unfolding pre-transition process (Fig. 5.6-4 C,D).

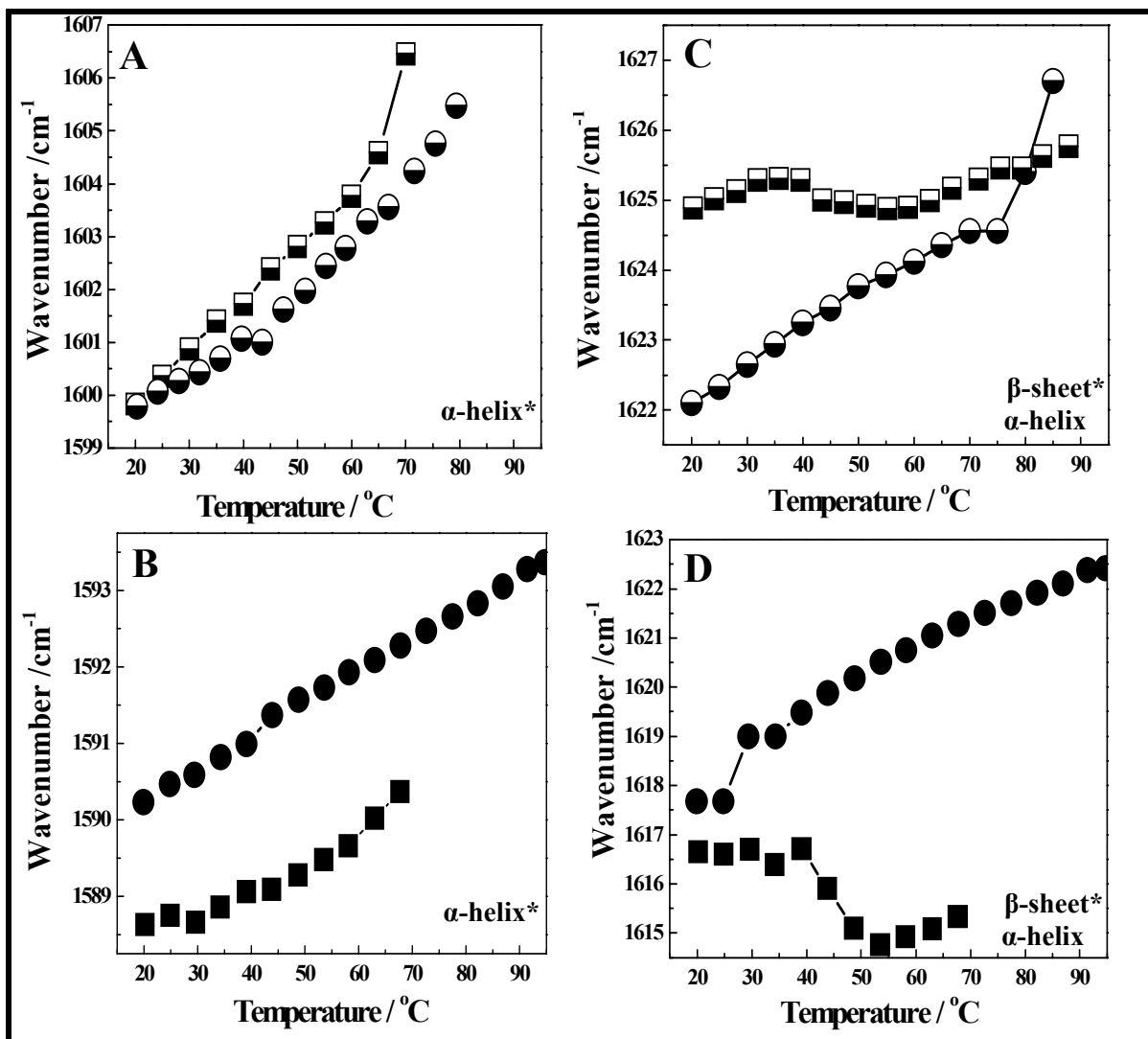


Figure 5.6-4 Temperature dependence plots for ^{13}C -Cen and ^{13}C -Cen/MLT complex for two Ca^{+2} concentrations. The closed symbols are for 4mM of CaCl_2 and the middle open symbols are for 0.2 mM of CaCl_2 : (A,B) α -helical maximum peaks in ^{13}C -Cen (circle) and complex (square), (C,D) ^{13}C -Cen (circle) and β -sheet* for ^{13}C -Cen (circle) and α -helix of MLT and β -sheet* peak combinations in the complex (square).

However, similar behavior was observed for MLT loop regions as a single component for the complex, suggesting no structural effect upon binding within the MLT loops (Figure 5.6-5).

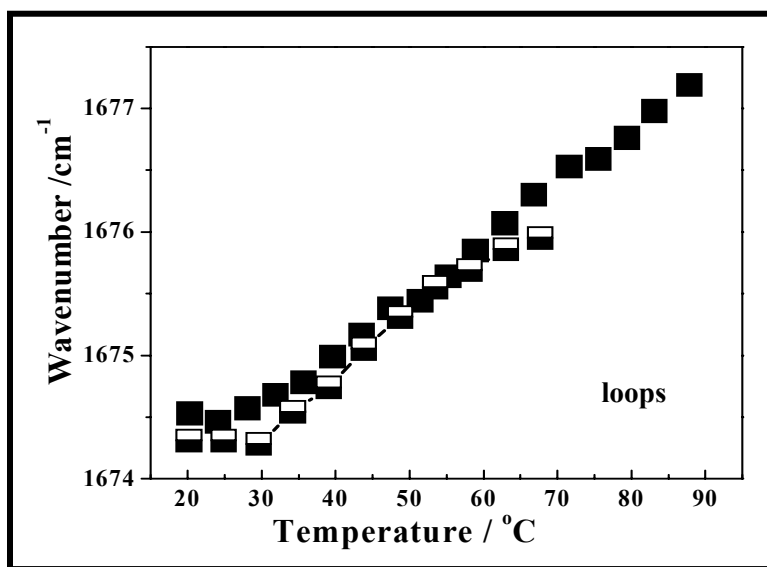


Figure 5.6-5 Temperature dependence plot of MLT loops region in the complex. Closed symbols are for 4mM of CaCl₂ and the middle open symbols are for 0.2 mM of CaCl₂.

5.7 Differential Scanning Calorimetry (DSC)

Differential scanning micro-calorimetry was used to determine the transition temperature for each protein and the protein complex during a thermal unfolding process in the presence of calcium. Figure 5.7-1 shows the thermograms obtained in the temperature range of 20-127 °C for ^{13}C -*Cen*, melittin, and the ^{13}C -*Cen*/MLT complex. Three pre-transitions were observed for ^{13}C -*Cen* at 30 °C, 60 °C, 81 °C, and a thermal denaturation transition temperature $T_m = 108$ °C in the presence of 4 mM CaCl_2 . In addition, melittin has a transition temperature at 64 °C and aggregation is observed at 100 °C. While, for ^{13}C -*Cen*/MLT complex a pre-transition temperature at 95 °C was observed. This transition would correspond to shifting of the third pre-transition observed for ^{13}C -*Cen* as a single component. Consequently, these results suggest that the presence of melittin stabilized ^{13}C -*Cen*.

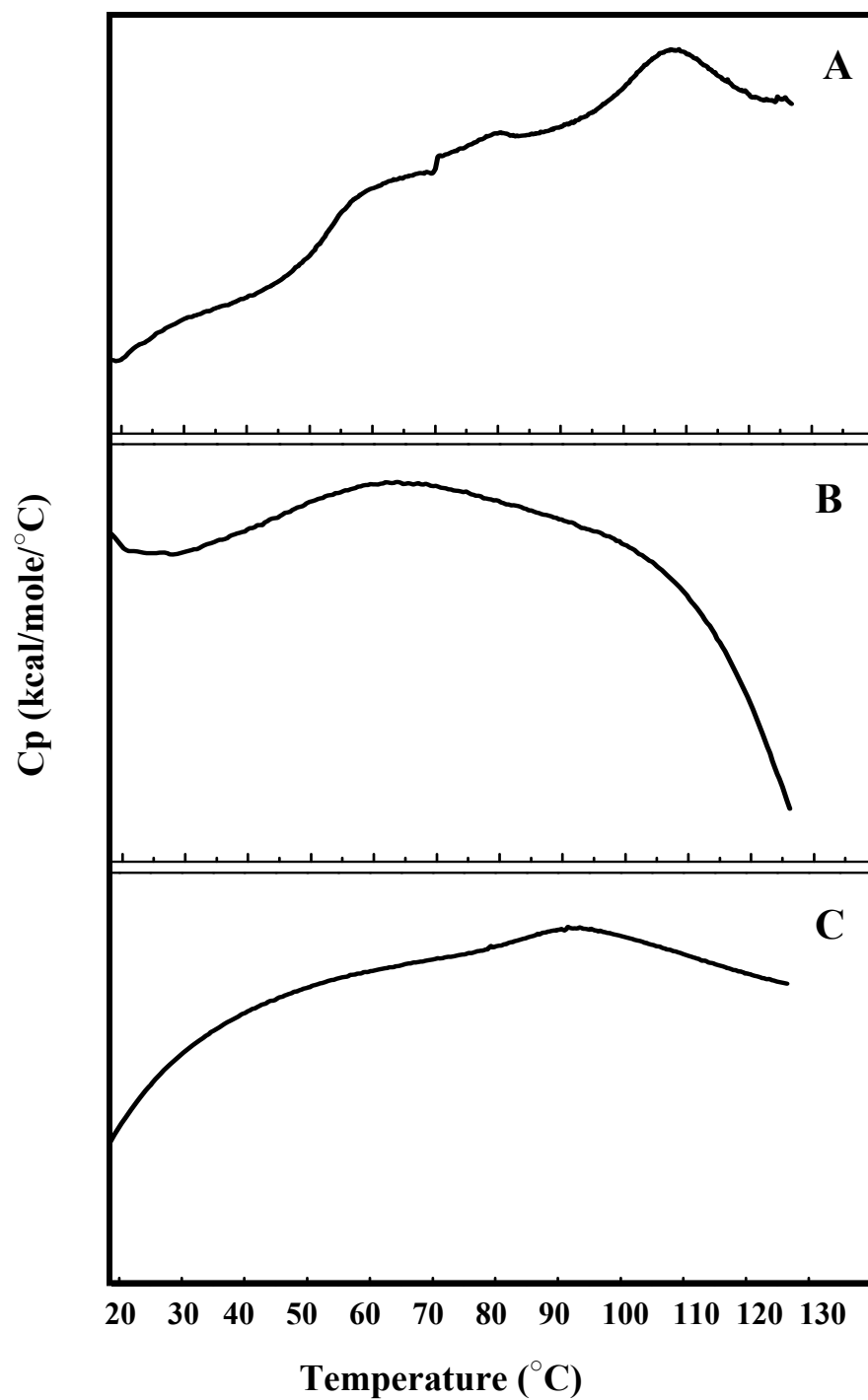


Figure 5.7-1 Thermograms of (A) ¹³C-Cen, (B) melittin and (C) ¹³C-Cen/MLT complex in the temperature range of 20 °C to 127 °C.

CHAPTER VI

CONCLUSIONS

6.1 Summary

The study of hydrogen/deuterium exchange of amide and exchangeable protons was important as a means of characterization of the solvent accessibility and dynamic structure properties of these proteins. In general, the exchange profile of amide II and II' bands (N-H & N-D deformation modes, respectively) in the ^{13}C -*Cen*/MLT complex contributions were established. Moreover, kinetic analysis for the complex was carried-out. A greater percent deuteration in the ^{13}C -*Cen*/MLT complex as compared to the single component (MLT or ^{13}C -*Cen*) and kinetic constants were determined during this process. The initial H→D exchange of the complex was governed by melittin.

On the other hand, the thermal perturbation study was useful for the characterization of relative stability and secondary structure variation induced by temperature changes. The variation of calcium concentrations was key for relative stability of ^{13}C -*Cen* and melittin in the complex and ^{13}C -*Cen* alone. Furthermore, the thermal dependence studies in the complex and ^{13}C -*Cen* as a single component, the interaction with melittin as well as calcium binding caused a greater stabilization during the thermal perturbation.

Also, two dimensional correlation analyses allowed enhancing of overlapping bands in the spectra and defined the sequence of events. Moreover, for both proteins the order of events obtained was random coil, loops, side chains, β -turns, and finally the α -helix.

Also, the DSC studies support the results obtained with FT-IR thermal dependence studies by corroborating the pre-transition temperatures for ^{13}C -Cen under varying conditions and in the centrin/melittin complex whereby stabilization of centrin was observed during the unfolding process.

6.2 Main conclusions

The determination of conformational changes and the extent of solvation were established for centrin, melittin as single components and the complex by using FT-IR spectroscopy. This method has proven useful for the study of protein complexes. The order of events served to describe the molecular changes leading up to the thermal denaturation and how the peptide stabilized centrin. The interaction within the protein complex, was driven by the effects on the α -helical motifs of centrin by MLT, to a greater extent than its interaction with calcium. This effect was also observed for the calorimetric studies whereby centrin pre-transition was shifted by 13 °C from 81 °C to 95 °C. Finally, these results provide the framework to study other centrin target peptides to further understand the biophysical and biochemical changes driving their interaction.

6.3 Future work

- Explore the interaction between ^{13}C -labeled *Chlamydomonas*, ^{13}C -Human centrin 1, and ^{13}C -Human 2 and Sfi1p, comprised of one centrin binding domain.

- Explore the interaction between ^{13}C -labeled *Chlamydomonas*, ^{13}C -Human centrin 1, and ^{13}C -Human 2 and Kar1p peptide.
- To determine dynamics, kinetics and relative thermal stability of these protein complexes and to compare with the results obtained with the model ^{13}C -Cen and melittin complex discussed in this thesis.

REFERENCES

Arrondo, J. L. and Goñi, F. (1999), "Structure and dynamics of membrane proteins as studies by infrared spectroscopy", *Biophysics and Molecular Biology*, vol 72, pp. 367-405.

Bornens, M. and Schiebel, E. (1995), "In search of a function for centrins", *Trends in cell Biology*, vol 5, pp. 197-201.

Comte, M, Maulet, Y. and Cox, J. A. (1983), "Ca²⁺ dependence high-affinity complex formation between calmodulin and melittin" *Biochemistry Journal*, vol 209, pp. 269-272.

Cox, J.A., Comte, M., Fitton, J.E. and DeGrado, W. F. (1985), "The interaction of calmodulin with amphiphilic peptides", *Journal of Biological Chemistry*, vol 260, pp. 2527-2534.

Cox, J. A., Tirone, F., Durussel, I., Firanescu, C., Blouquit, Y., Duchambon, P. and Craescu C. T. (2005), "Calcium and magnesium binding to human centrin 3 and interaction with target peptides", *Biochemistry*, vol 44, pp. 840-850.

Durussel, I., Blouquit, Y., Middendorp, S., Craescu, C.T. and Cox, J.A. (2000), "Cation and peptide binding properties of human centrin 2" *The FEBS Letter*, vol 472, pp. 208-12.

Fabian, H. and Mäntele, W., (2002), "*Infrared spectroscopy of proteins*", Encyclopedia analytical chemistry, ed John Wiley and Sons Ltd, pp. 1-25.

Fabian, H., Schultz, C., Naumann, D., Landt, O., Hahn, U. And Saenger, W. (1993), "Secondary structure and temperature-induced unfolding and refolding of ribonuclease T1 in aqueous solution: A Fourier transformed infrared spectroscopy study", *Journal of Molecular Biology*, vol 232, pp. 967-81.

Fisher, P. J., Prendergast, F. G., Ehrhardt, M.R., Urbauer, J. L., Wand, A. J., Sedarous, S. S., McCormick, D. J. and Buckley, P.J. (1994), "Calmodulin interacts with amphiphilic peptides composed of all D-amino acids", *Nature*, vol 368, pp. 651-653.

Gabel, F., Bicout, D., Lehnest, U., Tehei, M., Wiek, M. and Zaceai, G. (2002), "Protein dynamics studies by neutron scattering", *Review Biophysical*, vol 35, pp. 327-267.

<http://www.micromemananalytical.com/ATR-Ken/ATR.htm#FTIRlab>

<http://www.rcsb.org/pdb>

Horst R., Bertelsen E.B., Fiaux J., Wider G., Horwich A.L. and Wuthrich K. (2005), "Direct NMR observation of a substrate protein bound to the chaperon in GroEL", *Proceeding of the National Academy of Science USA*, vol 102, pp. 12748-53.

Hu, H., Sheehan, J. H. and Chazin, W.J. (2003), "Unique features in the C-terminal domain provide caltractin with target specificity", *Journal of Molecular Biology*, vol 330, pp. 473-484.

Hu, H., Sheehan, J. H. and Chazin, W.J. (2004), "The model of action of centrin: binding of Ca²⁺ and a peptide fragment of Kar1p to the C-terminal domain", *Journal of Cell Biology*, vol 48, pp. 123-135.

Hubner, W., Wong, P.T. and Mantsch, H.H. (1990), "The effect of hydrostatic pressure on the bilayer structure of phosphatidylcholines containing omega-cyclohexyl fatty acyl chains", *Biochemistry and Biophysical Acta*, vol 10027, pp. 229-37.

Jackson, M., Haris, P. I. and Chapman, D. (1989), "Fourier transform infrared spectroscopic studies of lipids, polypeptides and peptides", *Journal of Molecular Structure*, vol 214, pp. 329-355.

Jaspersen, S. J., Giddings, T. H. Jr. and Winey, M. (2002), "Mps3p is a novel component of the yeast spindle pole body that interacts with the yeast centrin homologue Cdc31p", *Journal of Cell Biology*, vol 159, pp. 945-956.

Kampl, M. D., Buckley, P., Yuan, P. and Prendergast, F. G. (1997), "Main chain and side chain dynamics of peptides in liquid solution from ¹³C NMR: Melittin as a model peptide", *Biochemistry*, vol 36, pp. 1678-1688.

Kilmartin, J. V. (2003), "Sfi1p has conserved centrin-binding sites and an essential function in budding yeast spindle pole body duplication", *Journal of Cell Biology*, vol 162, pp. 1211-1221.

Krimm, S. and Bandekar, J. (1986), "Vibrational spectroscopy and conformation of peptides, polypeptides and proteins", *Advances in Protein Chemistry*, vol 3, pp. 181-364.

Lavoie, H., Desbast, B., Vaknin, D. and Sallese, D. (2002), "Structure of rhodopsin in monolayers at the air-water interface: a PM-IRRAS and X-ray reflectivity study", *Biochemistry*, vol 41, pp. 13424-34.

Matei, E., Miron, S., Blouquit, Y., Duchambon, P., Durussel, I., Cox, J. A. and Craescu, C. T. (2003), "C-Terminal half of Human Centrin 2 Behaves like a regulatory EF-hand Domain", *Biochemistry*, vol 42, pp. 1439-1450.

Maulet, Y. and Cox, J.A. (1983), "Structural changes in melittin and calmodulin upon complex formation and their modulation by calcium", *Biochemistry*, vol 22, pp. 5680-5686.

- Noda, I. (1990), "Two-dimensional infrared (2D IR) spectroscopy: Theory and applications", *Applied Spectroscopy*, vol 44, pp. 550-561.
- Noda, I., Dowrey, A. E., Marcott, C., Story, M. and Ozaki, Y. (2000), "Generalized Two-dimensional correlation spectroscopy", *Applied Spectroscopy*, vol 54, pp. 236A-248A.
- Ortiz, M., Sanoguet, Z., Hu, H., Chazin, W. J., McMurray, C., Salisbury, J. L. and Pastrana-Rios, B. (2004), "Dynamics of hydrogen/deuterium exchange in Chlamydomonas Centrin", *Biochemistry*, vol 44, pp. 2409-2418.
- Pastrana-Rios, B. (2001), "Mechanism of unfolding of a model helical peptide", *Biochemistry*, vol 40, pp. 9074-9081.
- Pastrana-Ríos, B., Ocaña, W., Ríos M., Vargas, G. L., Ysa G., Poynter, G., Tapia, J. and Salisbury, J. L. (2002), "Centrin: its secondary structure in the presence and absence of cations", *Biochemistry*, vol 41, pp. 6911-6919.
- Pastrana-Rios, B., Teneva, S., Keough, K. M., Mautone, A. and Mendelshn, R. (1995), "External reflection absorption infrared spectroscopy study of lung surfactant protein SP-B and SP-C in phospholipids monolayers at the air/water interface", *Biophysical Journal*, vol 69, pp. 2531-40.
- Pearl F., Todd A., Sillitoe I., Dibley M., Redfern O., Lewis T., Bennett C., Marsden R., Grant A., Lee D., Akpor A., Maibaum M., Harrison A., Dallman T., Reeves G., Diboun I., Addou S., Lise S., Johnston C., Sillero A., Thornton J. and Orengo C. (2005), "The CATH Domain Structure Database and related resources Gene3D and DHS provide comprehensive domain family information for genome analysis", *Nucleic Acids Research*, vol 33, pp. D247-51.
- Perczel, A., Pank, K. and Fasman, G.D. (1992), "Decomposition of the circular dichroism spectra of the antiparallel beta sheet in proteins", *Proteins*, vol 13, pp. 57-69.
- Prestrelski, S.J., Byler, D.M. and Liebman, M.N., (1991), "Comparison of various molecular forms of bovine trypsin: correlation of infrared spectra with X-ray crystal structures", *Biochemistry*, vol 30, pp. 133-43.
- Raussens, V., Ruyschaert, J-M. and Goormanghtigh, E. (2004), "Analysis of 1H/2D exchange kinetics using model infrared spectra", *Applied spectroscopy*, vol 58, pp. 68-82.
- Salisbury, J. L. (1989), "Centrin and the alga flagellar apparatus", *Journal of Phycology*, vol 25, pp. 201-206.
- Salisbury, J. L. (1995), "Centrin, centrosomes, and mitotic spindle poles", *Current opinion in Cell Biology*, vol 7, pp. 39-45.

Salisbury, J. L., Suino, K. M., Busby, R. and Springett, M. (2002), "Centrin-2 is required for centriole duplication in mammalian cells", *Current Biology*, vol 12, pp. 1287-1292.

Salisbury, J. L. (2004), "Centrosomes: Sfi1p and Centrin unravel a structural riddle", *Current Biology*, vol 14, pp. R27-R29.

Schiebel, E. and Bornerns, M. (1995), „In search of a function for centrins", *Trends Cell Biology*, vol 5, pp. 197-201.

Shanmukh, S., Biswas, N., Waing, A. J., Walther, F.J., Wang, Z., Chang, Y., Notter, R. H. and Dluhy, R.A. (2005), "Structure and properties of phospholipids-peptide monolayer containing monomeric SP-B (1-25) II peptide conformation by IR spectroscopy", *Biophysics Chemistry*, vol 113, pp. 233-44.

Shifman, J.M. and Mayo, S.L. (2003), "Exploring the origins of binding specificity through the computational redesign of calmodulin", *Proceeding of the National Academy of Science USA*, vol 100, pp. 13274-13279.

Solomon, Berg and Martin (2002), "*Bology*", 5th edition.

Stahlberg, S. (2002), "Transmission Electron microscopy of proteins and proteins complex", *Thesis*. University Basel. Berlin.

Surewicz, W.K., Mantsch, H.H. and Chapman D. (1993), "Determination of protein secondary structure by Fourier transform infrared spectroscopy: a critical assessment", *Biochemistry*, vol 3, pp. 921-7.

Sutherland G.B.B.M. (1952), "Infrared analysis of the structure of aminoacids, polypeptides and proteins", *Advance in Protein Chemistry*, vol 5, pp. 291-318.

Tracewell, C. A., Cua, A., Bocian, D. F. and Brudvig, G. W. (2005), "Resonance Raman spectroscopy of carotenoid in Photosystem II core complexes", *Photosynthetic Research*, vol 83, pp. 45-52.

Venter, J. G., Lavy, S., Stockwell, T., Remington, K. and Halpern, A. (2003), "Massive parallelism randomness and genomics advances", *Nature Genetics*, vol 33, pp. 219-227.

Weaver, A. J., Kemple, M. D. and Prendergast, F. G. (1989), "Characterization of selectively ¹³C-labeled synthetic melittin and melittin analogues in isotropic solvents by Circular Dichroisms, Fluorescence, and NMR spectroscopy", *Biochemistry*, vol 28, pp. 8614-8623.

Weaver, A. J., Kemple, M. D., Brauner, J. W., Mendelsonhn, R. and Prendergast, F. G. (1992), "Fluorescence, CD, Attenuated Total Reflectance (ATR) FTIR, and ¹³C NMR characterization of the structure and dynamics of synthetic melittin and melittin analogues in lipid environments", *Biochemistry*, vol 31, pp. 1301-1313.

Weaver, C., Lee, V. D., Chaizin, W. J. and Huang, B. (1994), "High level expression in *Escherichia coli* and characterization of the EF₂ hand calcium-binding protein caltractin", *The Journal of Biological Chemistry*, vol 269, pp. 15795-15802.

Wiech, H., Geier, B. M., Paschke, T., Spang, A., Grein, K., Steinkötter, J., Melkonian, M. and Schiebel, E. (1996), "Characterization of Green Alga, Yeast, and Human Centris", *The Journal of Biological Chemistry*, vol 271, pp. 22453-22461.

Xu, Y., Oyola, R. and Gai, F. (2003), "Infrared study of the stability and folding kinetics of a 15-residues beta heparin", *Journal American Chemistry Society*, vol 125, pp. 15388-94.

Yang, J.T. (1996), "Prediction of protein secondary structure from amino acid sequence", *Journal of Protein Chemistry*, vol 2, pp. 185-91.